ISSN 0280-5316
ISRN LUTFD2/TFRT--5748--SE

Dynamic Simulation of the Train Concept Nowait Transit

Daria Madjidian
Arash Majedi

Department of Automatic Control
Lund Institute of Technology
May 2005

Department of Automatic Control
Lund Institute of Technology
Box 118
SE-221 00 Lund Sweden

Document name
MASTER THESIS

Date of issue
May 2005

Document Number
ISRNLUTFD2/TFRT--5748--SE

Author(s)
Daria Madjidian and Arash Majedi

Supervisor
Jan Tuszynski at Nowaittransit Group-Botnia Production AB
Stefan Solyom at Automatic Control in Lund

Sponsoring organization

Title and subtitle
Dynamic Simulation of the Train Concept Nowait Transit (Dynamisk simulering av tåg enligt Nowaittransit konceptet).

Abstract
This thesis deals with some aspects of the Nowait Transit train concept in order to provide insight and guidelines for further development. The train constitutes an interconnected closed string of cars and requires track areas with complex rail geometry. The thesis is divided into two parts where the first part provides a strategy in order to ensure smooth passing through these zones. The main part is dedicated to simplifying the stability analysis of the interconnected system. This is done by defining a stability criteria that can easily be applied to the subsystems and that guarantees the stability of the string. Simulation models are developed continuously throughout the thesis and are used to verify theoretical results and hypothesis.

Keywords

Classification system and/or index terms (if any)

Supplementary bibliographical information

ISSN and key title
0280-5316

ISBN

Language
English

Number of pages
50

Recipient's notes

Security classification

Acknowledgments

A number of persons have been of great importance for the completion of this thesis. In particular the contributions of Stefan Solyom and Jan Tuszynski deserve special credit. Also Dynasim and the Nowait Transit project group have provided valuable help concerning modeling problems. Finally we would like to thank the Department of Automatic Control for their kindness.

The development work behind this report was done partially in frames of the Vinnova project 2003-02103.

Contents

Abstract 1
Acknowledgments 2
1. Introduction 5
1.1 Background 5
1.2 Structure of the Nowait Transit train 5
1.3 Objectives 7
1.4 Terms and definitions 7
2. The Midi Model 8
2.1 A simplified model 8
2.2 Including rail dynamics and LIMs 9
2.3 Modeling and simulation in Dymola 12
3. The Macro model 16
3.1 String stability of the interconnected chain of cars 16
3.2 Interconnection of the cars 17
3.3 Exploiting the property of the transition zones 22
3.4 Observations 29
3.5 Verification of some of theory in Dymola 31
4. Conclusions 34
4.1 Problems and remarks 34
4.2 Suggestions for further development 35
A. Dymola models 36
A.1 Midi models 36
A.2 Macro models 43
B. Matlab scripts and Simulink Models 45
C. Converting rail data to functions 46
References 48

1. Introduction

1.1 Background

The idea of the *Nowait Transit* inner city train was developed originally by *Gert Andersson* and has recently entered a verification phase at *Botnia Production AB*, Örnsköldsvik, Sweden. The general concept of Nowait Transit is to achieve a high capacity and low cost mass transportation system. The main feature is that the cars constitute a closed chain that moves continuously, except for when major repairing has to be done. The train is assumed to operate more than 99 % of the time, ensuring passengers a "no wait" situation.

Since train acceleration and braking are the most energy consuming operations, the Nowait Transit train would be a low energy option compared to other mass transportation systems.

1.2 Structure of the Nowait Transit train

The cars are connected through *distance beams* of roughly the same length as the cars. The train runs continuously due to the folding and unfolding of the cars as they enter and leave the stations. See Figure 1.1. The car frequency, i.e. the number of cars that pass a point every second, is the same at all points on the track. The track consists of the four different kinds of sections listed below.

Straight section: This is similar to a regular train track. On this section the cars have a speed of 10 m/s.

Folding section: The track widens and forces the train to fold. The end of the folding section is located 4 m higher than the beginning of the section. This property transforms most of the kinetic energy to potential energy which will eventually be released in the unfolding section. The speed of the folding cars will decrease corresponding to the car effective length along the track. Final speed when entering the station will be approximately 1 m/sec.

Station section: This is the section where people step on and off the train. The train is maximally folded with an angle of approximately 85°. Folded cars fill the whole length of the platform and moving sidewalks along the platforms help passengers to embark and disembark the train.

Unfolding section: This is the opposite of the folding section. The cars head downhill from the station to the straight section and recover speed. The track narrows and the cars unfold.

The last three sections together are called the *transition region* or *transition zone*. The train is driven by *Linear Induction Motors* (LIMs), located

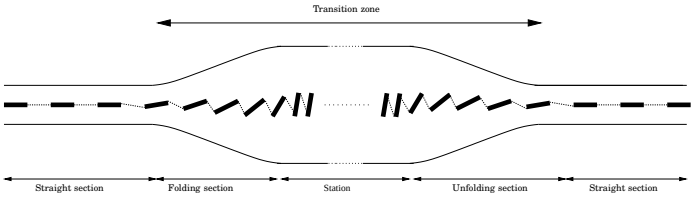

Figure 1.1 Different sections of the Nowait Transit Track

on the track. All cars have a reaction disc and when they pass over a LIM they are “pushed” with an induced force. Since no motor is attached to the car, the car complexity and weight is reduced. However, the disadvantages of the LIMs are; reduced efficiency in case of increased gap between the LIM and the reactor plate; and necessity of complex passing over control of a car moving between stationary LIMs. Also a sparse distance between the LIMs most likely involves problems. These properties are however outside of the scope of this thesis and all cars are assumed to have continuous contact with LIMs. A car has approximately a mass of 3000 kg and can carry a passenger load of another 2000 kg.

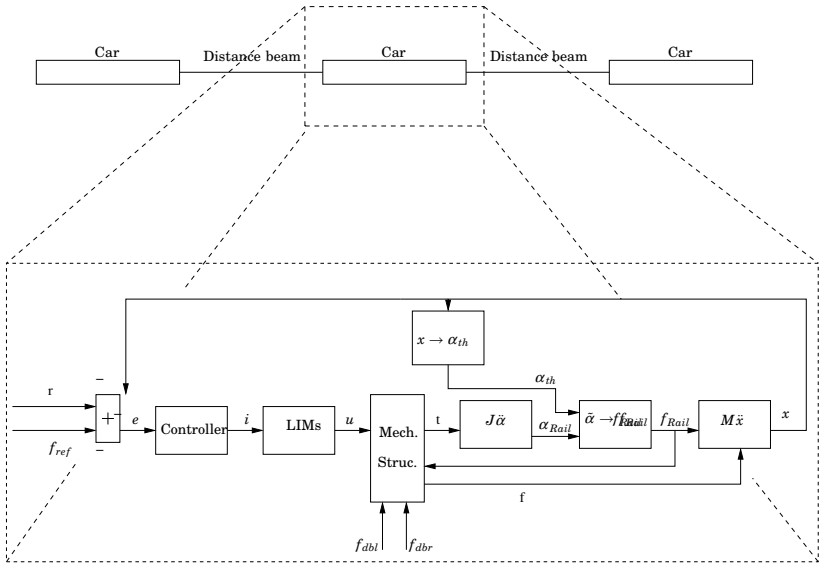

Figure 1.2 Block diagram showing the structure of the car model

The block diagram in Figure 1.2 shows the model structure of a single car interacting with adjacent cars. Internal car-rail forces affecting a car are gravity forces, f_{rail}, f_{dbl} and f_{dbr}. The two latter forces represent forces from the left and right distance beams respectively. The control forces are provided by the LIMs.

The controller objective is to provide a current to the LIMs in order to suppress effects of disturbances and to keep the forces acting on the track, f_{Rail}, equal to a desired reference force f_{ref}. This is needed in order to

avoid backlash between the car and the rails in the transition region. Furthermore it should force the car to maintain the desired position r on any point of the track.

The angle α_{th} in the figure is the angle calculated from the rail gauge at position x, i.e. the theoretical folding angle of the car. α_{Rail} is the actual folding angle. The block $J\ddot{\alpha}$ describes the rotating dynamics of a car and f_{Rail} is the perpendicular force of the rail constraint calculated form the angle deviation, $\tilde{\alpha} = \alpha_{th} - \alpha_{Rail}$, and rail wheel elasticity.

1.3 Objectives

The objectives of this work are the following:

1. To build Nowait Transit train models representing the dynamics of the cars moving on the track.
2. To suggest a control strategy for smooth car passage through the transition zone.
3. To suggest a control strategy ensuring stability of the whole string of interconnected cars.

1.4 Terms and definitions

Two kinds of models are developed in this thesis:

- **Midi models** representing a car moving through the transition zone.
- **Macro models** describing an interconnected set of cars, using simplified car models.

Both Midi and Macro models are studied using two different tools:

- Simplified models studied in Matlab/Simulink (www.mathworks.com).
- Detailed models studied in Dymola (www.dynasim.se).

Furthermore the following terms are used frequently in the report:

Transition zone: a region including the station, folding- and unfolding sections.

Distance beam: the beam that connects two cars.

LIM: Linear Induction Motor.

Closed chain: A chain of cars where all cars are connected to two adjacent cars.

Open chain: A chain of cars where the first and the last car are only connected to one car each.

2. The Midi Model

This chapter describes the Midi models used to analyze the rotational dynamics of a car. The models are built in three different complexity levels:

1. In Section 2.1 a simplified model is derived in order to give an understanding of the systems rotational dynamics due to the folding and unfolding of the cars.
2. In Section 2.2 a more detailed model is considered. This model includes the influence of the rail angles and the direction in which the LIMs act.
3. Section 2.3 moves the models into the Dymola environment allowing further model development of Section 2.2 by including nonlinearities and 3-dimensional forces acting on the cars.

The controller objective is to provide a current to the LIMs in order to suppress effects of disturbances and to keep the forces acting on the track, f_{Rail}, equal to a desired reference force f_{ref}. This is needed in order to reduce effects of backlash between the car and the rails.

2.1 A simplified model

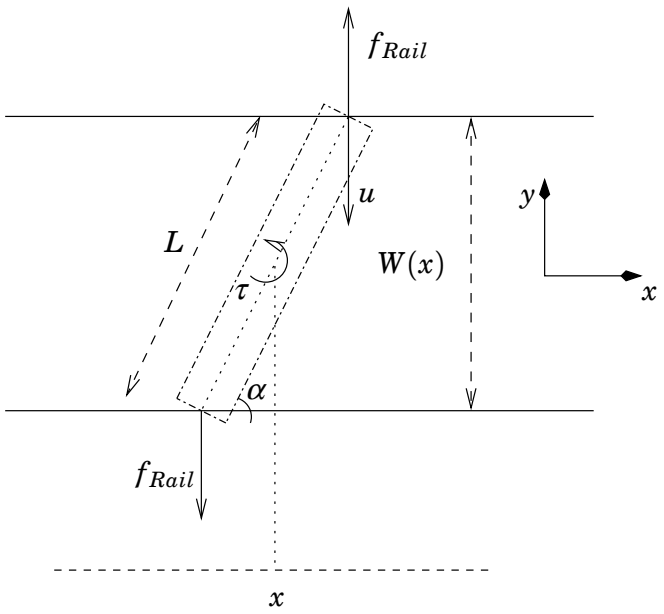

Figure 2.1 Forces acting on a car in a simplified model

This section provides a simple model of the rotating dynamics. The following assumptions have been made:

- Both rails are parallel to the track center line at all times and the rail gauge varies corresponding to a function $W(x)$.

- The resultant LIM force acts perpendicular to the upper rail.

Figure 2.1 shows a car on the track at position x and the forces acting on it. As it enters and leaves the transition region, the track gauge $W(x)$ varies, having a maximum width at the station and a minimum width on the straight section. The car is thus folded/unfolded an angle α depending on $W(x)$. The forces acting on each rail are given by f^u_{Rail} and f^l_{Rail} respectively and point outwards from the track center. The equations describing the rotation are given below:

$$\begin{cases} |f^u_{Rail}| = |f^l_{Rail}| = \frac{k}{2}(W - L\sin\alpha) \\ J\ddot{\alpha} = \frac{L}{2}\cos\alpha(f^u_{Rail} + f^l_{Rail} - u) - d\dot{\alpha} \end{cases}$$

where k describes the rail elasticity and d models rotational damping such as friction. The state space representation with $(x_1 \;\; x_2)^T = (\alpha \;\; \dot{\alpha})^T$ results in

$$\begin{cases} \dot{x_1} = x_2 \\ \dot{x_2} = \frac{1}{J}(\frac{L}{2}\cos x_1(k(W - L\sin x_1) - u) - dx_2) \\ f_{Rail} = k(W - L\sin x_1) \end{cases} \tag{2.1}$$

The equilibrium points of (2.1) are

$$(x^0_1 \;\; x^0_2)^T = \begin{cases} (\arcsin(\frac{kW^0 - u^0}{kL}) \;\; 0)^T \\ (\frac{\pi}{2} + n\pi \;\; 0)^T \qquad n = \ldots, -1, 0, 1 \ldots \end{cases}$$

where the first equilibrium point corresponds to the desired position of the car and the second equilibrium point to a position that should never occur since the track geometry allows a maximum car fold of less than 90^o. Figure 2.2 shows Simulink simulation results of α, f_{LIM}, $W(x)$ and f_{Rail} with a PID controller. 500 N has been used as reference. Note that the amplitude of the control signal is very high and that it alternates rapidly when the track width changes.

2.2 Including rail dynamics and LIMs

Figure 2.3 shows a car in the transition region together with the corresponding forces acting on it.The general equation describing the rotation of the car is

$$J\ddot{\alpha} = \tau_u + \tau_l - d\dot{\alpha}$$

where τ_u and τ_l are the torques on the car due to the forces from the rail and LIMs at the upper- and lower track respectively, and where d models rotational damping. Figure 2.4 shows all forces that yield torque on the car at the upper rail connecting point, and similarly Figure 2.5 shows the same at the lower rail connecting point.

From Figure 2.4 it is straightforward to derive τ_u:

$$\begin{aligned} \tau_u &= \frac{L}{2}\left(f^u_{Rail}\cos(\alpha - \beta^u) - f^u_{LIM}\cos(\frac{\pi}{2} - \alpha + \beta^u)\right) \\ &= \frac{L}{2}\left(f^u_{Rail}\cos(\alpha - \beta^u) - f^u_{LIM}\sin(\alpha - \beta^u)\right) \end{aligned}$$

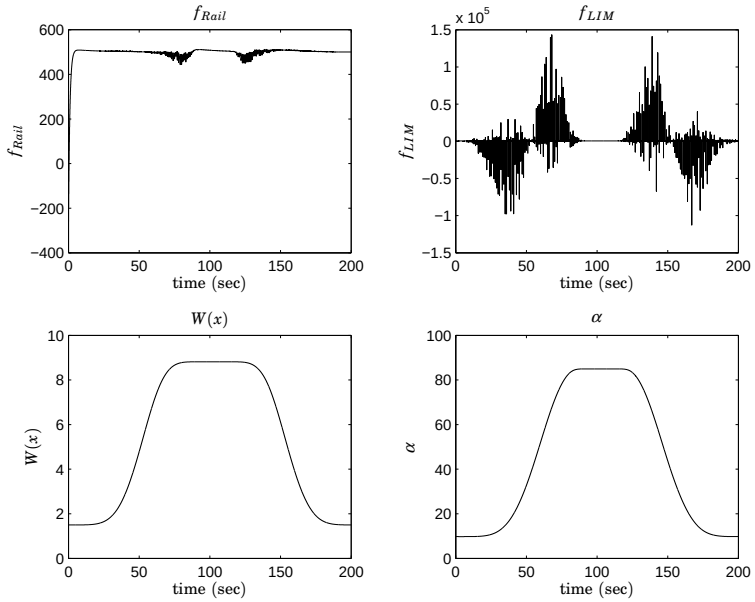

Figure 2.2 Simulation of the simple model with a PID-controller.

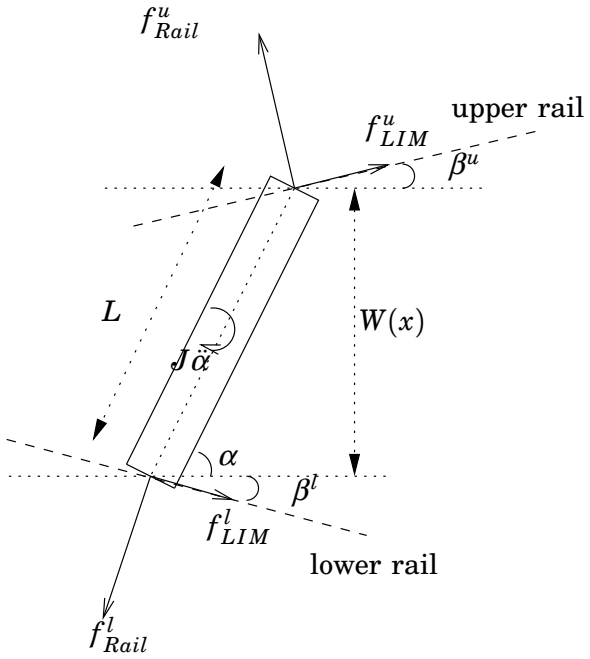

Figure 2.3 All forces acting on a single car in the transition zone

and similarly Figure 2.5 yields:

$$\tau_l = \frac{L}{2}\left(f^l_{Rail}\cos(\alpha+\beta^l) - f^l_{LIM}\cos(\frac{\pi}{2}-\alpha-\beta^l)\right)$$
$$= \frac{L}{2}\left(f^l_{Rail}\cos(\alpha+\beta^l) - f^l_{LIM}\sin(\alpha+\beta^l)\right).$$

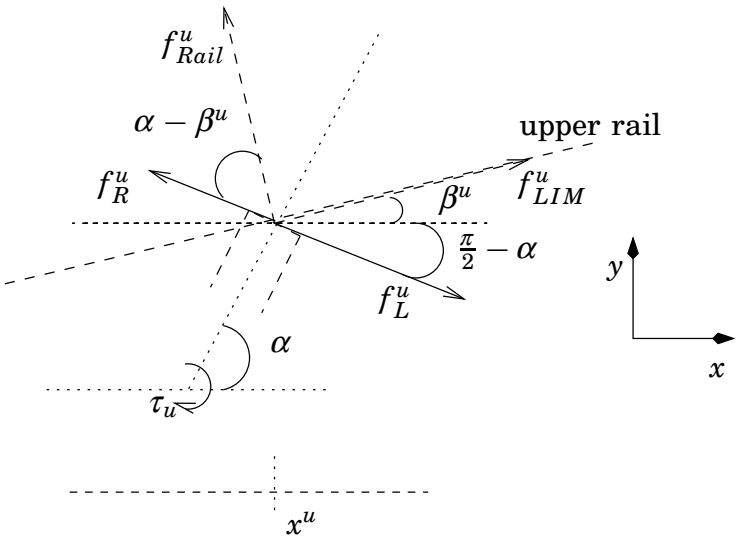

Figure 2.4 All forces acting on a single car at the upper rail connecting point

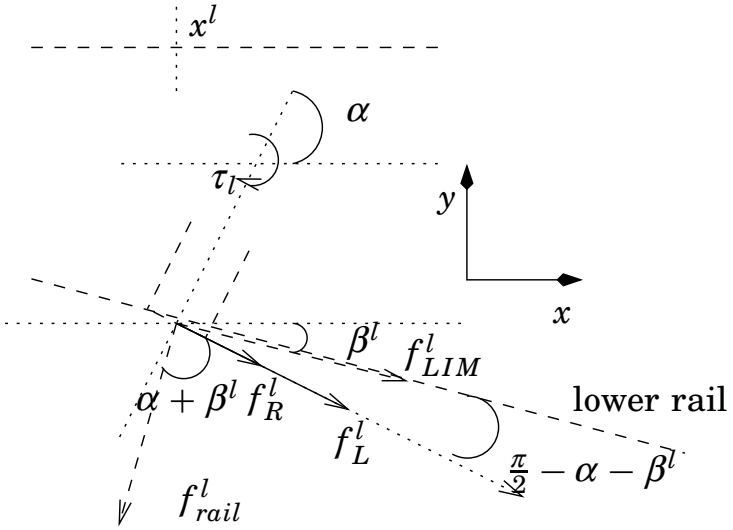

Figure 2.5 All forces acting on a single car at the lower rail connecting point

The total equation can now be written as:

$$J\ddot{\alpha} = \tau_u + \tau_l - d\dot{\alpha} = \frac{L}{2}\Big(f^u_{Rail}\cos(\alpha - \beta^u) - f^u_{LIM}\sin(\alpha - \beta^u) + f^l_{Rail}\cos(\alpha + \beta^l) + f^l_{LIM}\sin(\alpha + \beta^l)\Big) - d\dot{\alpha} \quad (2.2)$$

where $\beta^i = \arctan\left(\frac{d}{dx^i} g^i(x^i)\right)$ and where g^u and g^l describe the deviation along the y-axis of the upper and lower rails respectively. x^u and x^l are the positions of the upper- and lower connecting points of the car and the rail.

Due to the effect of the rail angles the expression for f^u_{Rail} and f^l_{Rail} will

take the following form:

$$\begin{aligned} f^u_{Rail} &= \frac{k}{2\cos\beta^u}(W - L\sin\alpha) \\ f^l_{Rail} &= \frac{k}{2\cos\beta^l}(W - L\sin\alpha) \end{aligned}$$

The equation system below describes all aspects of the model derived in this section.

$$\begin{cases} J\ddot{\alpha} = \frac{L}{2}\Big(f^u_r\cos(\alpha-\beta^u) - f^u_{LIM}\sin(\alpha-\beta^u) \\ +f^l_r\cos(\alpha+\beta^l) + f^l_{LIM}\sin(\alpha+\beta^l)\Big) - d\dot{\alpha} \\ f^u_{Rail} = \frac{k}{2\cos\beta^u}(W - L\sin\alpha) \\ f^l_{Rail} = \frac{k}{2\cos\beta^l}(W - L\sin\alpha) \\ \beta^u = \arctan(\frac{d}{dx^u}g^u(x^u)) \\ \beta^l = \arctan\left(\frac{d}{dx^l}g^l(x^l)\right) \end{cases}$$

2.3 Modeling and simulation in Dymola

The Nowait Transit car has been modeled in Dymola in cooperation with the Nowait Transit project group. Simulations have been made with a group of four such cars. For simplicity the cars run on a track whose geometry in the transition zone is based on simple cosine functions. The geometry of the track is displayed in Figure 2.6. The functions describing the rails are given by:

Upper track y-direction: $0.75 + (1 - 1.8664\cos(0.0698x^u))$.

Lower track z-direction: $1 - 1.8664\cos(0.0698x^u)$.

Lower track y-direction: $-0.75 - (1 - 1.8664\cos(0.0698x^l))$.

Lower track z-direction: $1 - 1.8664\cos(0.0698x^l)$.

The constants in the functions are based on knowledge of the track and are used in order to attain a realistic simulation environment. Methodology for adapting a real track to the model is presented in Appendix C.

Simulation of a group of cars

The purpose of the simulations is to animate a group of cars going into the transition region and reaching the station area. It should be noted that there are aspects that differ from the expected reality. First, the cars are not connected. The second aspect is that in order to simplify the control law, velocity control is used instead of position control. The velocity reference to the PID-controller is implemented as a function of the folding angle. It is designed in order to maintain a constant car frequency on any given point of the track, requiring approximately 9 m/sec on the straight section of the track and a velocity decrease to approximately 0.9 m/sec at the station.

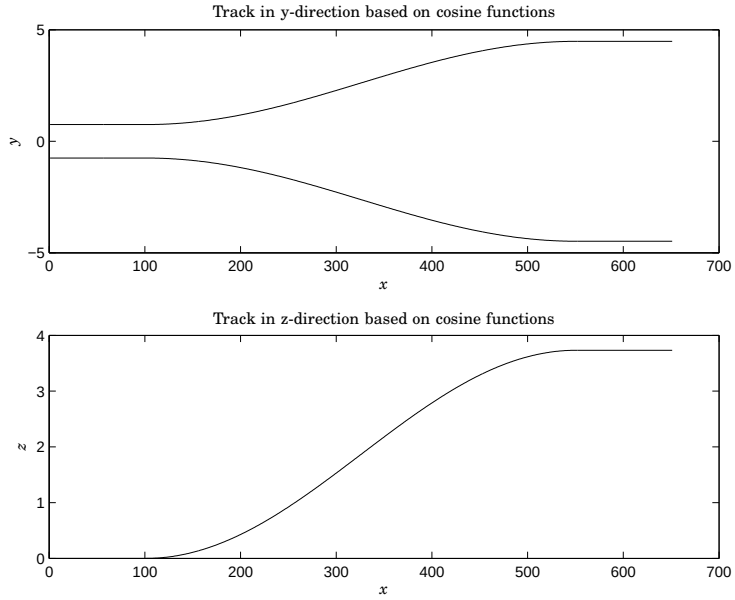

Figure 2.6 Track used in Dymola simulations

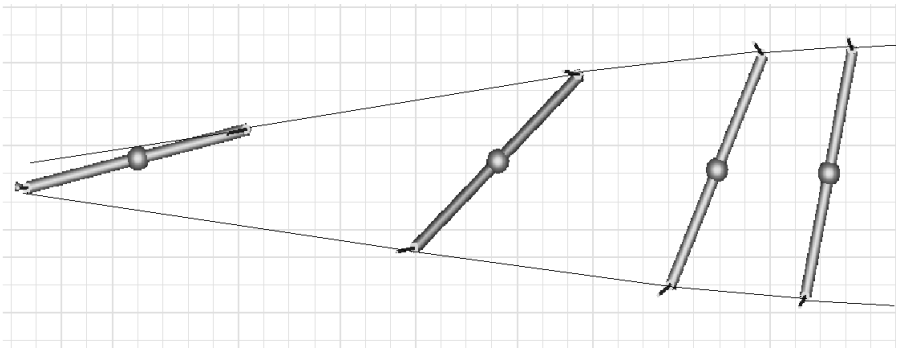

Figure 2.7 4 cars approaching the station area

Figure 2.7 below shows 4 wagons approaching the station.

Figure 2.8 shows the positions of the endpoints of the cars in y- and z-direction. Figure 2.9 displays the velocity and control signals.

Simulation of a force controlled car

As mentioned before the forces against the rail should be controlled in order to reduce undesired effects of backlash and to smooth accelerating/decelerating effects of the rail structure. If the connecting points of the car are not forced against the rail then even a small disturbance could cause the car to pound against the rail and reduce comfort for the passengers. Figure 2.10 shows the effects of force control with a PID controller. The reference was 500 N and both positive and negative impulse disturbances affected the upper rail connecting point directly. The velocity of the car was controlled as in the example above. The results show that force control clearly reduces the effects of backlash which can be seen in the number of zero crossings.

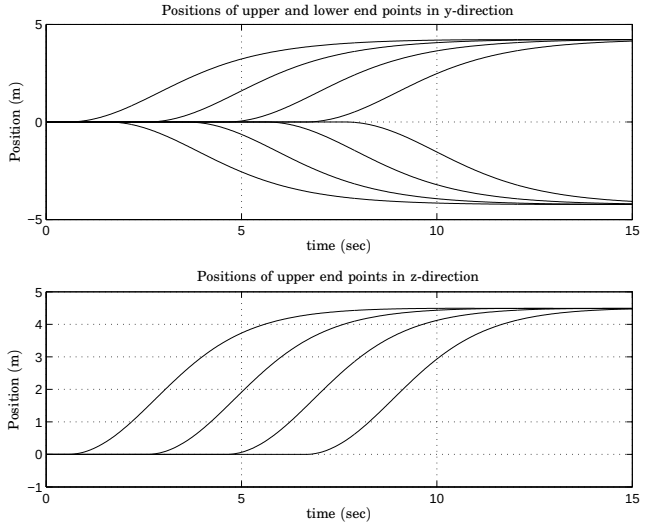

Figure 2.8 Upper plot: Position of the endpoints of the cars in y-direction. Lower plot: Position of the endpoints of the cars in z-direction.

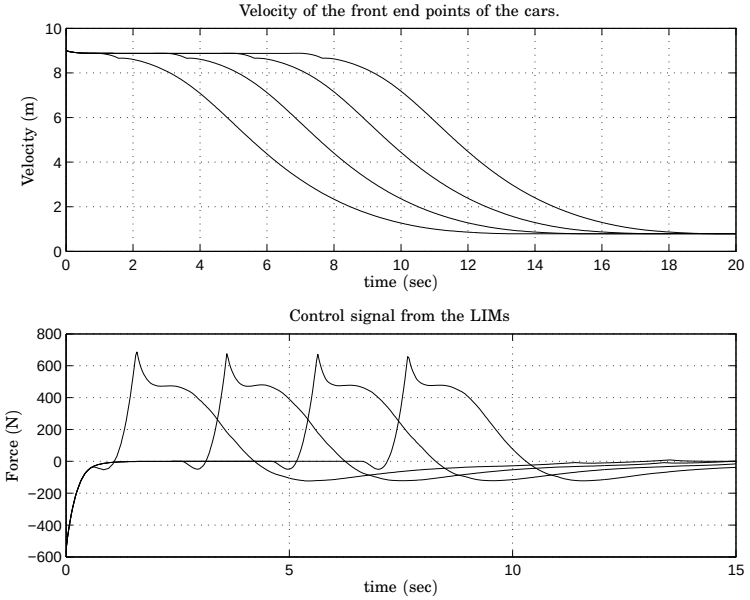

Figure 2.9 Upper plot: Velocity of the cars. Lower plot: Control signal

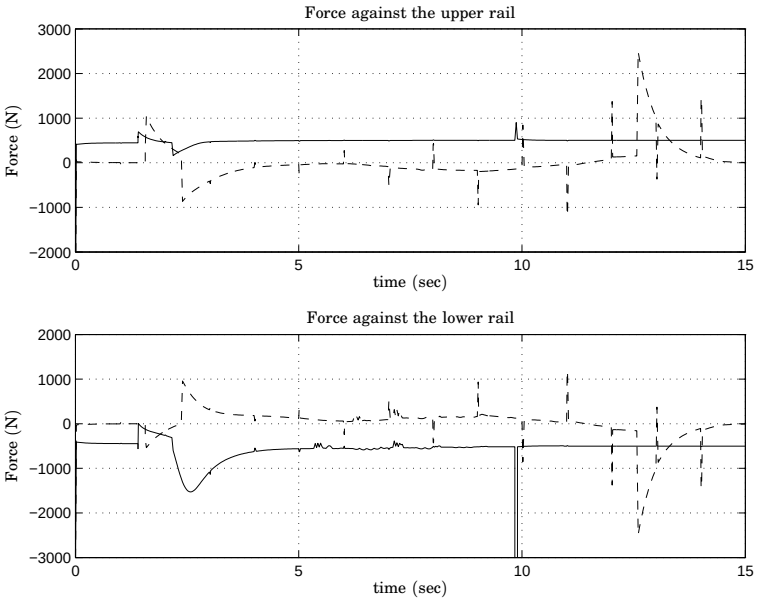

Figure 2.10 Simulation showing the effects of force control. Dashed: no control. Solid: with control.

3. The Macro model

The models in this chapter, called Macro models, deal with the interconnection of the cars. Section 3.1 introduces definitions for string stability of interconnected systems. Section 3.2 presents a model of a system, where the cars operate on a track without transition regions. Results will indicate a stability criteria presented in Section 3.4. Section 3.3 extends the model derived in 3.2 to include the transition regions. It will be shown that the properties of the transition zones can be used to simplify the stability analysis by dividing the interconnected system into subsystems. A theorem that guarantees string stability for these subsystems is then developed. Finally important observations based on simulation results are presented in Section 3.4. Conclusions of the above related to practical aspects are discussed in Chapter 4.

3.1 String stability of the interconnected chain of cars

The main requirement on the controller is that it guarantees asymptotic string stability of the interconnected system. The definition of string stability according to [1] is treated next.

Consider the system

$$\dot{x}^i = f(x^i, x^{i-1}, \ldots, x^{i-r+1}) \tag{3.1}$$

where $i \in \mathcal{N}$, $x^{i-j} \equiv 0 \ \forall i \leq j$, $x \in \mathcal{R}^n$, $f : \underbrace{\mathcal{R}^n \times \ldots \times \mathcal{R}^n}_{r \ times} \rightarrow \mathcal{R}^n$ and $f(0, \ldots, 0) = 0$.

DEFINITION 3.1
The origin of $\dot{x}^i = 0 \ i \in \mathcal{N}$ of (3.1) is string stable if given any $\rho > 0$, there exists $\delta > 0$ such that $||x^i(0)||_\infty < \delta \Rightarrow \sup_i ||x^i(\cdot)||_\infty < \rho$. □

DEFINITION 3.2
The origin of $\dot{x}^i = 0 \ i \in \mathcal{N}$ of (3.1) is asymptotically string stable if it is string stable and $x^i(t) \rightarrow 0$ asymptotically for all $i \in \mathcal{N}$. □

REMARK 3.1
For the system under consideration string stability can be summarized as the following: if the (bounded) state of a car does not cause an unrestrained growth of any other car state in the system, it is string stable. Furthermore if all states go to the origin it is asymptotically string stable. If all cars are (asymptotically) string stable the interconnected system is (asymptotically) string stable. □

Introduce $\varepsilon^i = x_1^{i-1} - x_1^i$ as the relative displacement between car $i-1$ and i. If all cars are identical, then

$$\varepsilon^i(s) = G_\varepsilon(s)\varepsilon^{i-1}(s) + G_\varepsilon(s)\varepsilon^{i+1}(s) \tag{3.2}$$

where $G_\varepsilon(s)$ is the displacement transfer function between neighboring cars.

Although no condition has been found mathematically to guarantee asymptotic string stability for a closed chain, the simulation results that follow in the subsequent sections provide a clear indication of such a condition on $||G_\varepsilon||_\infty$. A condition for string stability of an open chain is presented in Section 3.3.

3.2 Interconnection of the cars

The Macro model will initially describe an interconnected chain of cars on a straight track i.e, a track without transition zones. Assuming that the distance beam is elastic, the interconnected cars operating on a rail of constant gauge, can be modeled as masses that are connected through a damped spring.

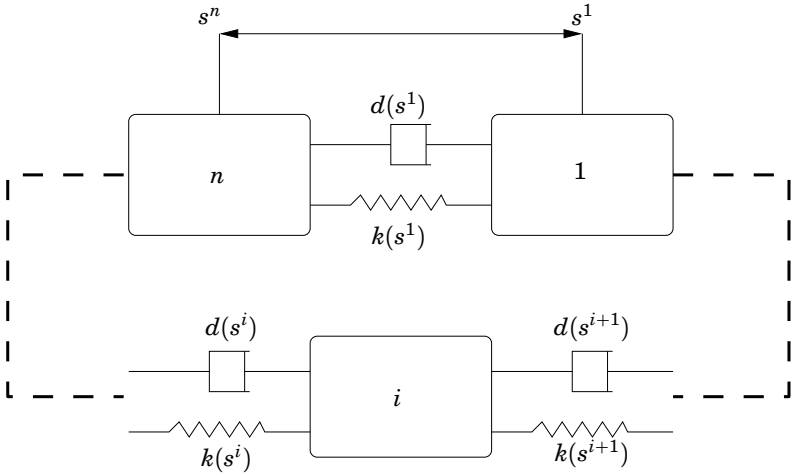

Figure 3.1 An interconnected string of cars

Figure 3.1 illustrates how a car i at position s^i interacts with its neighbors, car $i-1$ and $i+1$, at positions s^{i-1} and s^{i+1} respectively. s^i is to be considered as the deviation of the center of car i from its starting position. The cars move clockwise as in Figure 3.1. The interconnection spring (distance beam) has spring constant k, spring damping d and d^* models the environmental damping such as friction.

Now defining

$$\begin{aligned} x_1^i &= s^i \\ x_2^i &= \dot{s}^i \\ u &= F_{LIM} \end{aligned}$$

the equation describing the interconnection of a car with its neighbors is given by:

$$\dot{x}_2^i = k(x_1^{i-1} + x_1^{i+1}) + d(x_2^{i-1} + x_2^{i+1}) - 2kx_1^i - (2d + d^*)x_2^i + u^i. \qquad (3.3)$$

The Laplace transform of (3.3) yields

$$X_1^i(s) = G_x(s)(X_1^{i-1}(s) + X_1^{i+1}(s)) + G_u(s)U^i(s)$$

where

$$\begin{aligned} G_x(s) &= \frac{ds+k}{ms^2+(2d+d^*)s+2k} \\ G_u(s) &= \frac{1}{ms^2+(2d+d^*)s+2k} \end{aligned} \tag{3.4}$$

and the propagation error is

$$\varepsilon^i(s) = X_1^{i-1}(s) - X_1^i(s) = \underbrace{G_x(s)}_{G_\varepsilon(s)}(\varepsilon_{i-1}+\varepsilon_{i+1}) + G_u(s)(U^{i-1}(s)-U^i(s)). \tag{3.5}$$

The state space representation of a single car i is given by

$$\underbrace{\begin{pmatrix} \dot{x}_1^i \\ \dot{x}_2^i \end{pmatrix}}_{\dot{x}^i} = \underbrace{\begin{pmatrix} 0 & 1 \\ -\frac{2k}{m} & -\frac{2d+d^*}{m} \end{pmatrix}}_{A^1} \underbrace{\begin{pmatrix} x_1^i \\ x_2^i \end{pmatrix}}_{x^i} +$$

$$+ \underbrace{\begin{pmatrix} 0 & 0 \\ \frac{k}{m} & \frac{d}{m} \end{pmatrix}}_{A^2} \left(\underbrace{\begin{pmatrix} x_1^{i-1} \\ x_2^{i-1} \end{pmatrix}}_{x^{i-1}} + \underbrace{\begin{pmatrix} x_1^{i+1} \\ x_2^{i+1} \end{pmatrix}}_{x^{i+1}} \right) + \underbrace{\begin{pmatrix} 0 \\ \frac{1}{m} \end{pmatrix}}_{B^1} u^i, \tag{3.6}$$

and in larger scale, representing n connected cars

$$\begin{pmatrix} \dot{x}^1 \\ \dot{x}^2 \\ \dot{x}^3 \\ \vdots \\ \dot{x}^i \\ \vdots \\ \dot{x}^{n-1} \\ \dot{x}^n \end{pmatrix} = \begin{pmatrix} A^1 & A^2 & 0 & & \dots & & 0 & A^2 \\ A^2 & A^1 & A^2 & 0 & \dots & & & 0 \\ 0 & A^2 & A^1 & A^2 & 0 & \dots & & \vdots \\ \vdots & \ddots & & \ddots & & \ddots & & \\ \vdots & & & A^2 & A^1 & A^2 & & \vdots \\ & & & & & \ddots & & \\ 0 & & \dots & & 0 & A^2 & A^1 & A^2 \\ A^2 & 0 & & \dots & & 0 & A^2 & A^1 \end{pmatrix} \begin{pmatrix} x^1 \\ x^2 \\ x^3 \\ \vdots \\ x^i \\ \vdots \\ x^{n-1} \\ x^n \end{pmatrix}$$

$$+ \overbrace{\begin{pmatrix} B^1 & & \\ & \ddots & \\ & & B^1 \end{pmatrix}}^{n\ blocks} \begin{pmatrix} u^1 \\ \vdots \\ u^n \end{pmatrix} = Ax + Bu. \tag{3.7}$$

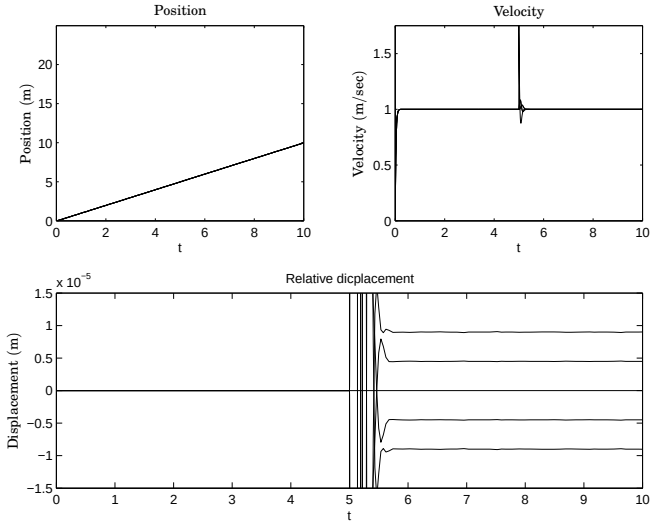

Figure 3.2 Simulation result obtained when using PI-velocity control.

Controlling car velocity with a PI-controller

One approach in controlling the interconnected string would be to try to maintain the desired velocity for each car at all times. A PI-controller for each car is given by:

$$\begin{aligned} u^i &= K_r(v - x_2^i) + x_3^i \\ \dot{x}_3^i &= \frac{Kr}{Tr}(v - x_2^i) \end{aligned}$$

where v^i is the velocity reference of car i.

A problem that arises when applying velocity control is that no consideration is given to the displacement between the cars. This system is string stable but not asymptotically string stable since, even if the velocity of all cars are made equal, constant forces applied by the LIMs could still give rise to undesirable distances between the cars. This can be seen in the stationary gain of $G_\varepsilon(s)$.

$$\begin{aligned} \varepsilon_i(s) &= \underbrace{\frac{sd + k}{ms^2 + s(K + d^* + 2d) + K/T_i + 2k}}_{G_\varepsilon(s)}(\varepsilon_{i-1}(s) + \varepsilon_{i+1}(s)) \\ \Rightarrow \quad G_\varepsilon(0) &= \frac{k}{K/Ti + 2k} \neq 0 \end{aligned}$$

Figure 3.2 shows the car positioning, velocity and the relative displacement error of five cars with a disturbance in velocity after 5 sec.

Controlling car positioning with a PI^{2}D-controller

A natural approach would now be to use a PI^{2}D-controller with a double integrator to control the car positioning. The double integrator is needed in order to follow a ramp in the reference signal. The controller equations

are given by:

$$\begin{aligned} u^i &= K_r(r - x_2^i) + x_4^i \\ \dot{x}_3^i &= \frac{Kr}{Tr}(r - x_1^i) \\ \dot{x}_4^i &= x_3^i. \end{aligned}$$

where r^i is the position reference of car i.

Recall that the displacement between car $i-1$ and i is defined as $\varepsilon^i = x_1^{i-1} - x_1^i$. Its Laplace transform is given by

$$\begin{aligned} \varepsilon^i(s) &= \frac{ds^3 + ks^2}{ms^4 + (2d + d^* + K_r T_d)s^3 + (2k + K_r)s^2 + \frac{K_r}{T_i}} \Big(\varepsilon^{i-1}(s) + \varepsilon^{i+1}(s) \Big) \\ &+ \frac{Kr(T_d s^3 + s^2 + 1/T_i)}{ms^4 + (2d + d^* + K_r T_d)s^3 + (2k + K_r)s^2 + \frac{K_r}{T_i}} \underbrace{\Big(r^{i-1}(s) - r^i(s) \Big)}_{0}. \end{aligned}$$

In order to attain an asymptoticly stable system the poles of the transfer function have to be placed in the closed left half plane.

$$ms^4 + (2d + d^* + K_r T_d)s^3 + (2k + K_r)s^2 + \frac{K_r}{T_i} = (s^2 + 2\zeta_1\omega_1 s + \omega_1^2)(s^2 + 2\zeta_2\omega_2 s + \omega_2^2).$$

The resulting equation system is given by

$$\begin{aligned} 2d + d^* + K_r T_d &= 2m(\zeta_1\omega_1 + \zeta_2\omega_2) \\ 2k + K_r &= m(\omega_1^2 + \omega_2^2 + 4\zeta_1\zeta_2\omega_1\omega_2) \\ 0 &= 2m\omega_1\omega_2(\zeta_1\omega_2 + \zeta_2\omega_1) \qquad (3.8) \\ \frac{K_r}{T_i} &= m\omega_1^2\omega_2^2 \qquad (3.9) \end{aligned}$$

According to (3.9) $\omega_1 \neq 0$ and $\omega_2 \neq 0$ as long as the loop is closed. Then according to (3.8) $\zeta_1 = 0$ and $\zeta_2 = 0$ and that makes it impossible to attain an asymptotically stable system with a PI^2-controller.

Controlling car positioning with a PII^{2}D-controller

By applying the control law:

$$u^i(s) = \left(K_r + \frac{Kr}{sT_i} + \frac{K_r}{s^2 T_{ii}} + K_r s T_d \right) e^i(s).$$

where $e^i(t) = r^i - x_1^i$, G_ε takes the following form:

$$G_\varepsilon = \frac{ds^3 + ks^2}{ms^4 + (2d + d^* + K_r T_d)s^3 + (2k + K_r)s^2 + \frac{K_r}{T_i}s + \frac{K_r}{T_{ii}}}$$

The following parameter solutions are obtained:

$$\begin{aligned} K_r &= -2\,k + m{\omega_1}^2 + m{\omega_2}^2 + 4\,m\zeta_1\,\zeta_2\,\omega_1\,\omega_2 \\ T_i &= -1/2\,\frac{2\,k - m{\omega_1}^2 - m{\omega_2}^2 - 4\,mz_1\,\zeta_2\,\omega_1\,\omega_2}{m\omega_1\,\omega_2\,\left(\zeta_1^1\,\omega_2 + \zeta_2\,\omega_1\right)} \\ T_{ii} &= -\frac{2\,k - m{\omega_1}^2 - m{\omega_2}^2 - 4\,m\zeta_1\,\zeta_2\,\omega_1\,\omega_2}{m{\omega_1}^2{\omega_2}^2} \\ T_d &= -\frac{-d^* + 2\,mz_1\,\omega_1 + 2\,m\zeta_2\,\omega_2 - 2\,d}{2\,k - m{\omega_1}^2 - m{\omega_2}^2 - 4\,m\zeta_1\,\zeta_2\,\omega_1\,\omega_2} \end{aligned}$$

The simulation results are presented in Figure 3.3.

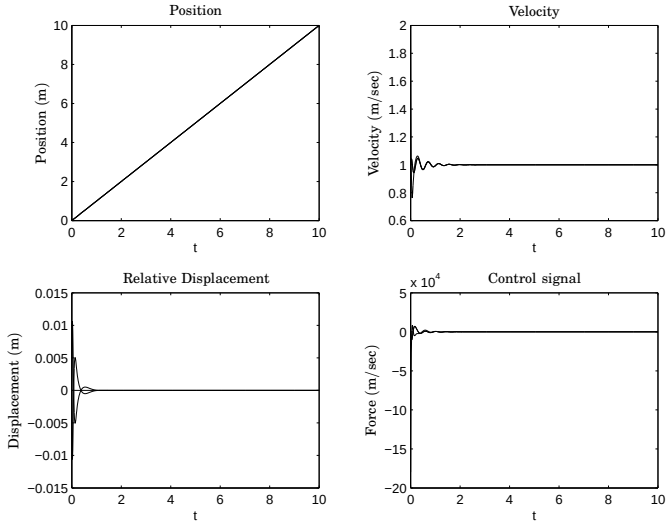

Figure 3.3 Simulation with a PII^{2}D-controller.

Simulation results are shown in Figure 3.3. Observations indicate that the system is string stable if $||G_\varepsilon(iw)||_\infty \leq \frac{1}{2}$. Although no proof is given for the closed chain case, a proof is derived for the open chain in Section 3.3.

Global state feedback control

Another approach would be to use a global state feedback controller. As in the previous position control cases the controller has to include a double integrator. Note that this approach requires global state information, i.e. state information of all cars.

Since this approach is straightforward only the simulation results will be presented. In Figure 3.4 the poles of the overall system are placed in -2. String stability is thus not an issue.

Local state feedback control

Another way to control the interconnected system is to apply state feedback for each car. The advantage versus global state feedback is that in order to control one car, state information from other cars is not needed. This requires less computational power. The disadvantage is that changes

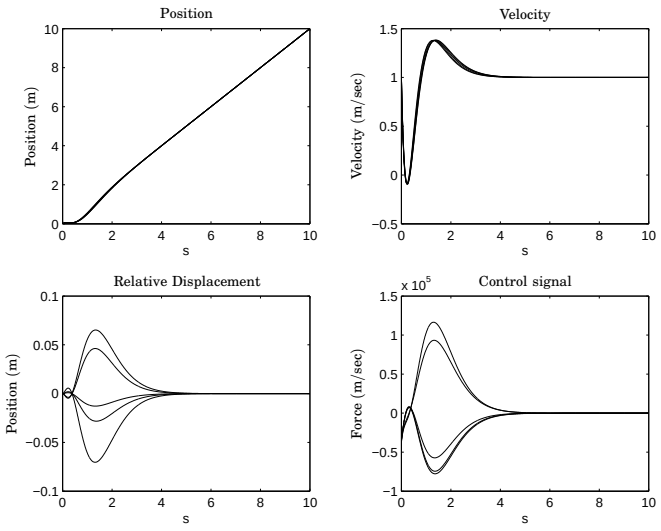

Figure 3.4 Simulation with a global state feedback controller.

in other parts of the chain can not be anticipated, since the state information of all cars is not known.

As in previous cases two extra integrating states are introduced. The closed loop system for a single car is given by:

$$\dot{x}^i = \underbrace{(A^1 - B^1 L)}_{\hat{A}^1} x^i + \underbrace{(B^r + B^1 l_r)}_{\hat{B}^1} r + A^2 x^{i\pm 1}$$

where

$$\hat{A}^1 = \begin{pmatrix} 0 & 1 & 0 & 0 \\ -\frac{2k+l_1}{m} & -\frac{d^*+2d+l_2}{m} & -\frac{l_3}{m} & -\frac{l_4}{m} \\ -1 & 0 & 0 & 0 \\ 0 & 0 & 1 & 0 \end{pmatrix}, \hat{B}^1 = \begin{pmatrix} 0 \\ \frac{l_r}{m} \\ 1 \\ 0 \end{pmatrix}, \quad \hat{A}^2 = A^2. \tag{3.10}$$

The displacement transfer function is given below.

$$G_\varepsilon(s) \quad = \quad \frac{s^3 d + s^2 k}{m s^4 + s^3(d^* + 2d + l_2) + s^2(l_1 + 2k) - s l_3 - l_4}$$

Figure 3.5 shows a simulation with an initial velocity deviation. The poles of each subsystem are placed on the real axis in -17 and $||G_\varepsilon||_\infty \approx 0.3$.

Simulations indicate that the system is string stable if $||G_\varepsilon||_\infty \leq \frac{1}{2}$.

3.3 Exploiting the property of the transition zones

When considering the transition zone, one can see that the coupling coefficients, d and k, will depend on the angle between the car itself and the

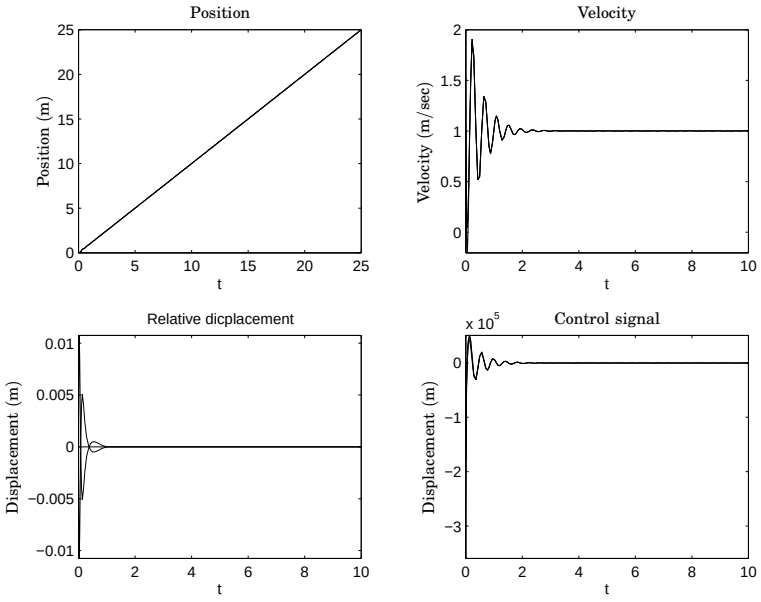

Figure 3.5 Simulation with a local state feedback controller.

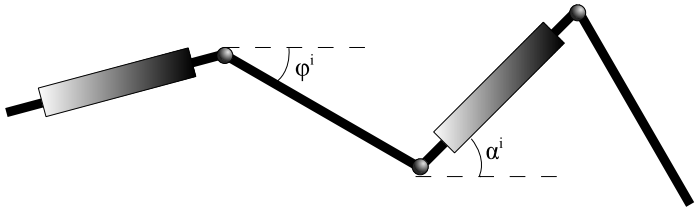

Figure 3.6 A car attached to two distance beams.

two distance beams attached to it (Figure 3.6). The system can still be represented as in (3.7) with coupling coefficients:

$$\begin{aligned} k^i &= k\cos^2(\varphi^i) \\ d^i &= d\cos^2(\varphi^i) \end{aligned}$$

where the dynamics of φ are given by

$$L_d\cos\varphi^i = x_1^i - x_1^{i-1} - \frac{L}{2}\Big(\cos(\alpha^{i-1}) + \cos(\alpha^i)\Big) \tag{3.11}$$

and where L_d is the length of the distance beam.

The above equations result in a system of the same form as (3.7) with the

following changes:

$$\begin{pmatrix} \dot{x}^1 \\ \dot{x}^2 \\ \dot{x}^3 \\ \vdots \\ \dot{x}^i \\ \vdots \\ \dot{x}^{n-1} \\ \dot{x}^n \end{pmatrix} = \begin{pmatrix} A^1 & A^{1+} & 0 & & \dots & & 0 & A^{1-} \\ A^{2-} & A^2 & A^{2+} & 0 & \dots & & & 0 \\ 0 & A^{3-} & A^3 & A^{3+} & 0 & \dots & & \vdots \\ \vdots & \ddots & & \ddots & & \ddots & & \\ \vdots & & & A^{i-} & A^i & A^{i+} & & \vdots \\ & & & & & \ddots & & \\ 0 & & \dots & & 0 & A^{(n-1)-} & A^{n-1} & A^{(n-1)+} \\ A^{n+} & 0 & & \dots & & 0 & A^{n-} & A^n \end{pmatrix} \begin{pmatrix} x^1 \\ x^2 \\ x^3 \\ \vdots \\ x^i \\ \vdots \\ x^{n-1} \\ x^n \end{pmatrix}$$

$$+ \overbrace{\begin{pmatrix} B^1 & & \\ & \ddots & \\ & & B^1 \end{pmatrix}}^{n\ blocks} \begin{pmatrix} u^1 \\ \vdots \\ u^n \end{pmatrix} \tag{3.12}$$

$$\begin{cases} A^i = \begin{pmatrix} 0 & 1 \\ -\frac{k}{m}(\cos^2\varphi^{i-1} + \cos^2\varphi^i) & -\frac{d}{m}(\cos^2\varphi^{i-1} + \cos^2\varphi^i) - \frac{d^*}{m} \end{pmatrix} \\ A^{i-} = \cos^2\varphi^{i-1} \begin{pmatrix} 0 & 0 \\ \frac{k}{m} & \frac{d}{m} \end{pmatrix} \\ A^{i+} = \cos^2\varphi^i \begin{pmatrix} 0 & 0 \\ \frac{k}{m} & \frac{d}{m} \end{pmatrix} \\ B^1 = \begin{pmatrix} 0 \\ \frac{1}{m} \end{pmatrix} \end{cases}$$

Effects of the transition zones

Since one rail loop includes a number of transition zones, and since in every such zone several cars are folded maximally at the same time, that is α near 90°, the stability analysis can be simplified. If the dynamics of φ are not considered in the system then it is a linear time varying system. Since the coupling coefficients are small (they are multiplied with $\cos^2\varphi$), almost no forces can propagate through the transition zones. However if *no control* is applied, $||G_\varepsilon||_\infty$ in the transition region increases as α grows. This can be seen in Figure 3.7 where $||G_\varepsilon||_\infty$ is plotted against φ together with the resonance frequency of $G_\varepsilon(i\omega)$.

The result displayed in Figure 3.7 is due to the fact that, the damping of G_ε decreases with an increasing φ which leads to a high resonance peak. This can also be seen in the denominator of (3.4):

$$ms^2 + (d^{i-1} + d^i + d^*)s + k^{i-1} + k^i = ms^2 + 2\zeta\omega s + \omega^2.$$

where ζ is the damping and ω is the resonance frequency. By applying appropriate control the resonance peak can easily be damped.

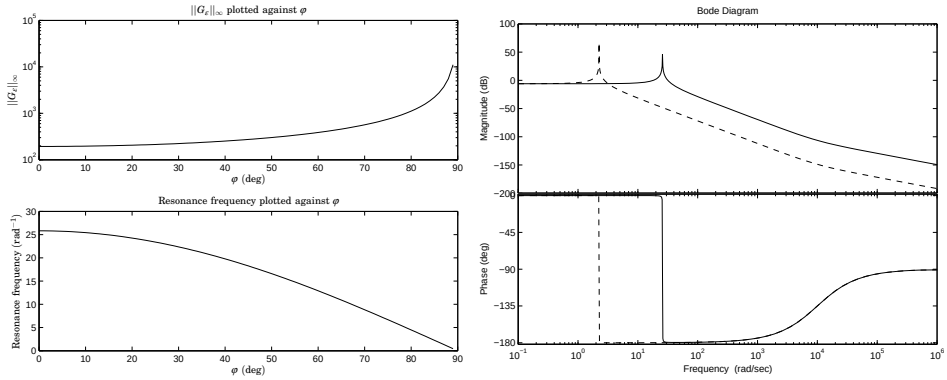

Figure 3.7 Upper left plot:$||G_\varepsilon||_\infty$ plotted against φ. Lower left plot: The resonance frequencies of the systems against φ. Right plot: The bode plot for $\varphi = 0^\circ$ (solid) and $\varphi = 85^\circ$ (dashed).

In Figure 3.8 a control signal is shown in the case of φ =0^o and φ=85^o. In both cases sections with three cars are simulated for $||G_\varepsilon||_\infty \approx 6 \cdot 10^{-3}$ and an initial displacement of 0.1 m on the first car. The control force shown belongs to the second car. The folded system obviously requires a smaller control signal to maintain its position. By applying controllers in the transition region that make $||G_\varepsilon||_\infty$ sufficiently small, the error propagation through a number of cars with enough folding will be negligible. This makes it justifiable to model such regions as breaks in the chain.

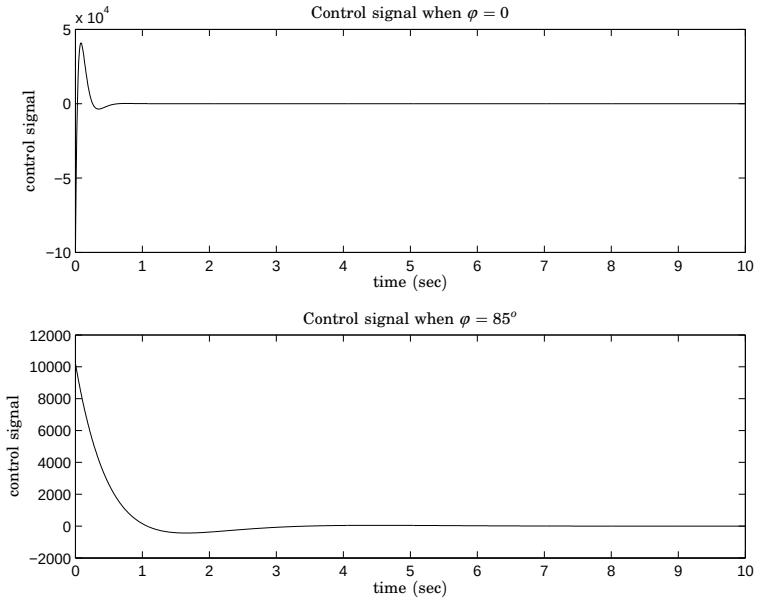

Figure 3.8 The control signals of two systems. Upper plot: $\varphi = 0$. Lower plot: $\varphi = 85^o$. In both plots $r = 3$, $||G_\varepsilon||_\infty \approx 6 \cdot 10^-3$ and an initial displacement of 0.1 m is given to the systems.

String stability of the interconnected open chain of cars

Using the observation of the previous section, cars on different sides of a transition region can not affect one another (given appropriate controllers

in the transition region). The interconnected system is thus broken into sections as shown in Figure 3.9. For simplicity it is assumed that $\varphi = 0$. A section gives rise to a system of the same form as in (3.7):

$$\begin{pmatrix} \dot{x}^1 \\ \dot{x}^2 \\ \dot{x}^3 \\ \vdots \\ \dot{x}^i \\ \vdots \\ \dot{x}^{r-1} \\ \dot{x}^r \end{pmatrix} = \begin{pmatrix} \tilde{A}^1 & A^2 & 0 & & \dots & & 0 & 0 \\ A^2 & A^1 & A^2 & 0 & \dots & & & 0 \\ 0 & A^2 & A^1 & A^2 & 0 & \dots & & \vdots \\ \vdots & \ddots & & \ddots & & \ddots & & \\ \vdots & & & A^2 & A^1 & A^2 & & \vdots \\ & & & & & \ddots & & \\ 0 & & \dots & & 0 & A^2 & A^1 & A^2 \\ 0 & 0 & & \dots & & 0 & A^2 & \tilde{A}^1 \end{pmatrix} \begin{pmatrix} x^1 \\ x^2 \\ x^3 \\ \vdots \\ x^i \\ \vdots \\ x^{r-1} \\ x^r \end{pmatrix}$$

$$+ \overbrace{\begin{pmatrix} B^1 & & \\ & \ddots & \\ & & B^1 \end{pmatrix}}^{r \text{ blocks}} \begin{pmatrix} u^1 \\ \vdots \\ u^r \end{pmatrix} \tag{3.13}$$

where A^1,A^2 and B^1 are the same as in (3.6), r is the number of cars in a section, and where

$$\tilde{A}^1 = \begin{pmatrix} 0 & 1 \\ -\frac{k}{m} & -\frac{d+d^*}{m} \end{pmatrix}.$$

The fact that $\tilde{A}^1$ only contains one $\frac{k}{m}$- and $\frac{d}{m}$ element as in contrast to A^1 in (3.6) is due to the fact that the first and last car in the section, are only connected to one car each. For the same reason the corner A^2 matrices that appear in (3.7) are zero in (3.13).

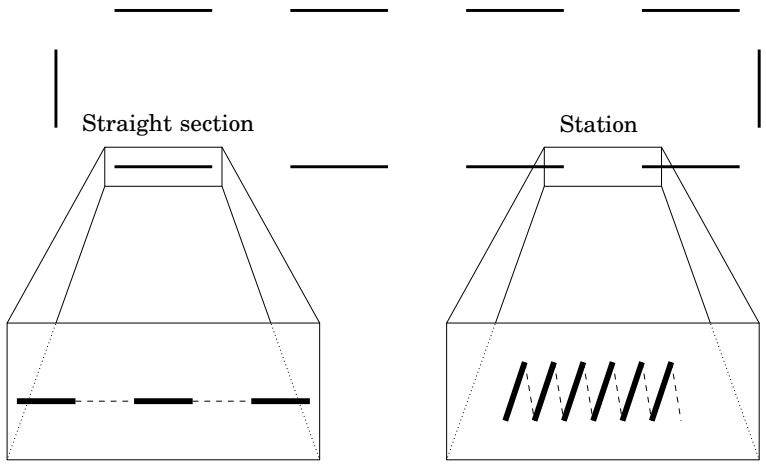

Figure 3.9 The transition regions are modeled as breaks

A stability criteria for broken chain sections will now be derived. By stabilizing the subsystems, the overall system with transition regions should

also be stabilized since maximum error propagation between two cars occurs when they are on the straight region of the track. *Note that this is only true in the case where appropriate controllers are employed in order to make* $||G_\varepsilon||_\infty$ *sufficiently small in regions where the cars are maximally folded*. Special consideration should thus be given to the design of the controllers in the transition zone.

Let $G_2(s) = G_\varepsilon(s)$, where $G_\varepsilon(s)$ is the displacement propagation transfer function between two cars. Then the following set of equations describe the displacement propagation between the cars in a section.

$$\begin{aligned} \varepsilon^2 &= G_2\varepsilon^3 \\ \varepsilon^3 &= G_2\varepsilon^2 + G_2\varepsilon^4 \\ &\vdots \\ \varepsilon^{r-1} &= G_2\varepsilon^{r-2} + G_2\varepsilon^r \\ \varepsilon^r &= G_2\varepsilon^{r-1} \end{aligned} \tag{3.14}$$

This gives rise to

$$\frac{\varepsilon^i}{\varepsilon^{i+1}} = G_i = \frac{G_2}{1 - G_2 G_{i-1}}$$

String stability is guaranteed if

$$||G_i||_\infty < 1, \forall i = 2, \ldots, r-1 \tag{3.15}$$

and no unstable even modes (unstable pole-zero cancellations) are present.

The task is now to find a condition for $||G_2||_\infty$ such that (3.15) is guaranteed.

LEMMA 3.1
Given a function

$$f(x, y) = \frac{x}{1 - xy}.$$

If $0 < x \leq \frac{1}{2}$ and $0 < y < 1$, then $f(x, y) < 1$. □

PROOF 3.1

$$f'(x, y) = \frac{\partial f}{\partial x} + \frac{\partial f}{\partial y} = \frac{1 - xy - x(-y)}{(1 - xy)^2} + \frac{x^2}{(1 - xy)^2} = \frac{1 + x^2}{(1 - xy)^2} > 0.$$

Since f in monotonously increasing in it's arguments, $f(x, y) < f(\frac{1}{2}, 1) = 1$. □

THEOREM 3.1
$||G_i||_\infty < 1$, $i = 2, \ldots, n$, $n \to \infty$ iff $||G_2||_\infty \leq \frac{1}{2}$. □

PROOF 3.2—PROOF OF SUFFICIENCY
For some i it yields that

$$||G_i||_\infty = \left|\left|\frac{G_2}{1-G_2G_{i-1}}\right|\right|_\infty \leq \frac{||G_2||_\infty}{1-||G_2||_\infty||G_{i-1}||_\infty}$$

Let $||G_2||_\infty < \frac{1}{2}$. Then it follows directly from lemma 3.1 that

$$\begin{aligned} ||G_3||_\infty &\leq \frac{||G_2||_\infty}{1-||G_2||_\infty||G_2||_\infty} < 1 \\ ||G_4||_\infty &\leq \frac{||G_2||_\infty}{1-||G_2||_\infty||G_3||_\infty} < 1 \\ &\vdots \\ ||G_i||_\infty &\leq \frac{||G_2||_\infty}{1-||G_2||_\infty||G_{i-1}||_\infty} < 1 \end{aligned}$$

□

PROOF 3.3—PROOF OF NECESSITY

$$||G_i||_\infty \leq \frac{||G_2||_\infty}{1-||G_2||_\infty||G_{i-1}||_\infty} < 1 \Rightarrow ||G_2||_\infty < \frac{1}{1+||G_{i-1}||_\infty}$$

Assuming the worst case scenario:

$$||G_{i-1}||_\infty = 1-\delta \Rightarrow ||G_2||_\infty < \frac{1}{2-\delta}$$

where δ is an arbitrary small positive number. As $\delta \to 0$, $||G_2||_\infty \leq \frac{1}{2}$. □

REMARK 3.2
In the case of a finite number of cars the restriction on $||G_2||_\infty$ is relaxed. In order to attain $||G_i||_\infty < 1$ in general, $||G_2||_\infty < \mu(n)$ where $\frac{1}{2} \leq \mu(n) < 1$ depending on the number of cars n. □

The stability margin with respect to $||G_2||_\infty$ is shown in Figure 3.10 for sections where the number of cars differ.

Applying Theorem 1 in order to obtain string stability

Theorem 1 in Section 3.3 guarantees string stability for a broken chain of interconnected cars if the cars are stable themselves, i.e. the system representing an unconnected car must have all poles in the left half plane. In order to avoid erroneous results when using this theorem as a stability criteria, it is of crucial importance to make certain that the maximum amplification for displacement propagation ($||G_\varepsilon||_\infty$) between cars in the transition zone is negligible. Special care should thus be given to ensure that all controllers that are to operate in the transition region fulfill this requirement.

The question of which car should be considered as the first or last car in a section is not relevant as long as $||G_\varepsilon||_\infty \leq \frac{1}{2}$ between all cars, and $||G_\varepsilon||_\infty$

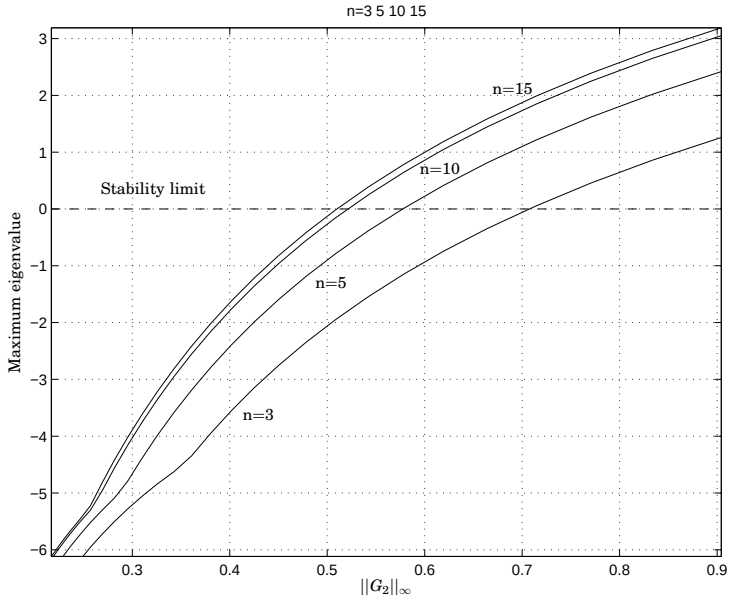

Figure 3.10 Stability margin plotted against $||G_2||_\infty$ for sections with 3, 5, 10 and 15 cars.

is sufficiently small between cars with maximum folding. It is important to remember that in order to obtain string stability an unconnected car itself must be stable. If these requirements are met then the overall system is string stable.

Figure 3.11 shows simulation for a section with $r = 10$ cars and $||G_\varepsilon||_\infty = 0.4913$ between each car. The system is obviously stable. In Figure 3.12 the same system has been simulated with $||G_\varepsilon||_\infty = 0.5249$ which results in an unstable system.

3.4 Observations

During the simulations a number of observations have been made. **Note that these observations are based entirely on Matlab simulations**.

1. The following equality seems to hold:

$$||G_i||_\infty = \frac{||G_2||_\infty}{1 - ||G_2||_\infty ||G_{i-1}||_\infty}$$

   This can be a very useful approximation since Matlab does not seem to be able to calculate $||\frac{G_2}{1-G_2G_{i-1}}||_\infty$ directly as i increases.

   For example the following results have been obtained. **Method 1** corresponds to $||\frac{G_2}{1-G_2G_{i-1}}||_\infty$ and **method 2** corresponds to $\frac{||G_2||_\infty}{1-||G_2||_\infty||G_{i-1}||_\infty}$. Results are shown for two different cases of system parameters. Local state feedback controllers have been used and the poles of each subsystem have been placed in p.

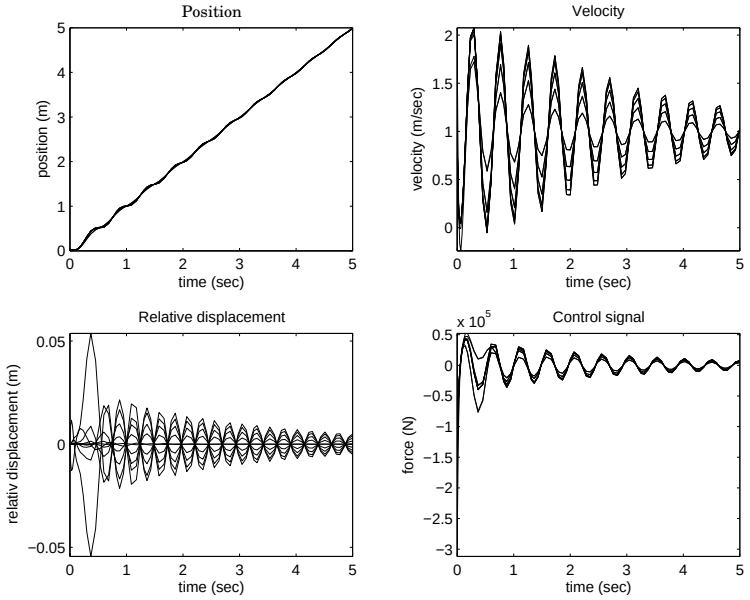

Figure 3.11 Simulation results for a section of 10 cars with $||G_\varepsilon||_\infty = 0.4913$. The system is string stable.

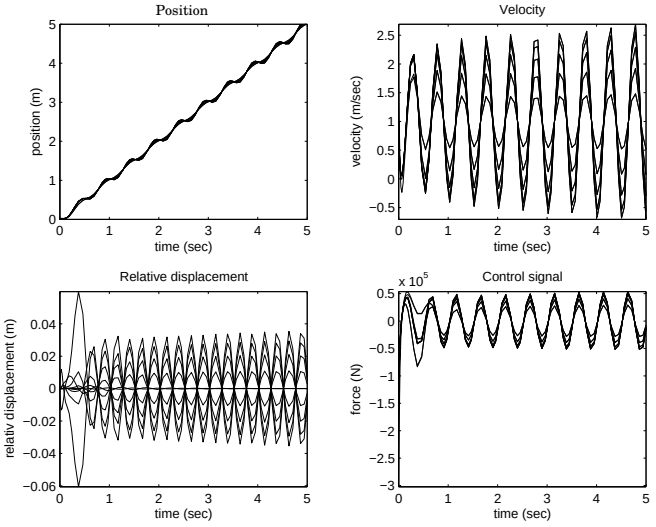

Figure 3.12 Simulation results for a section of 10 cars with $||G_\varepsilon||_\infty = 0.5249$. The system is not string stable.

n	5
k	1e4
d	1e1
d^*	0
m	3e3
p	-1.3

$\Rightarrow$

i	Method 1	Method 2
1	0.4931	0.4931
2	0.6515	0.6515
3	0.7265	0.7265
4	0.7683	0.7683

n	4
k	1e4
d	1e2
d^*	0
m	3e3
p	-4.3

$\Rightarrow$

i	Method 1	Method 2
1	0.4507	0.4507
2	0.5656	0.5656
3	0.6049	0.6049

2. An open interconnected system is stable if:

$$\prod_{i=1}^{n-1} ||G_i||_\infty < 1.$$

See Figure 3.13. Given that this is true, condition 3.15 can be relaxed.

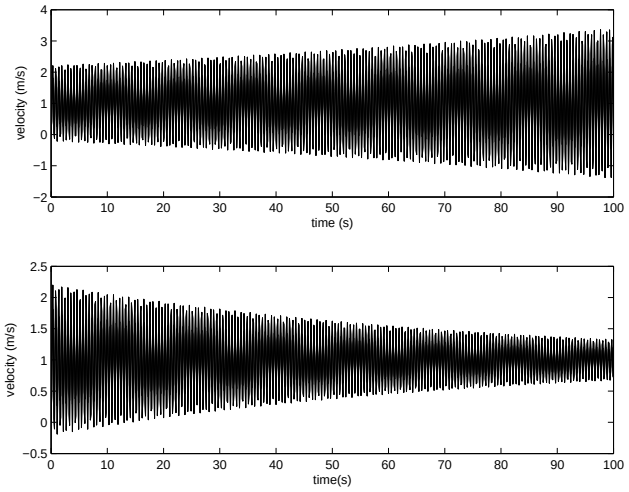

Figure 3.13 $\prod_{i=1}^{n-1} ||G_i||_\infty = 1.0114$ in the upper plot. $\prod_{i=1}^{n-1} ||G_i||_\infty = 0.9790$ in the lower plot

3. The considered *closed* interconnected system is stable, regardless of the number of cars, as long as:

$$||G_\varepsilon||_\infty \leq \frac{1}{2}$$

See Figure 3.14.

3.5 Verification of some of theory in Dymola

In this section some Dymola plots (See Appendix A.2) are provided in order to verify the theory derived in the above sections, already confirmed by Matlab simulations. Figure 3.15 shows a stable and an unstable case for an open chain of three cars. Figure 3.16 displays similar results for a closed chain of three cars. In all cases $||G_\varepsilon||_\infty$ is chosen such that the systems are

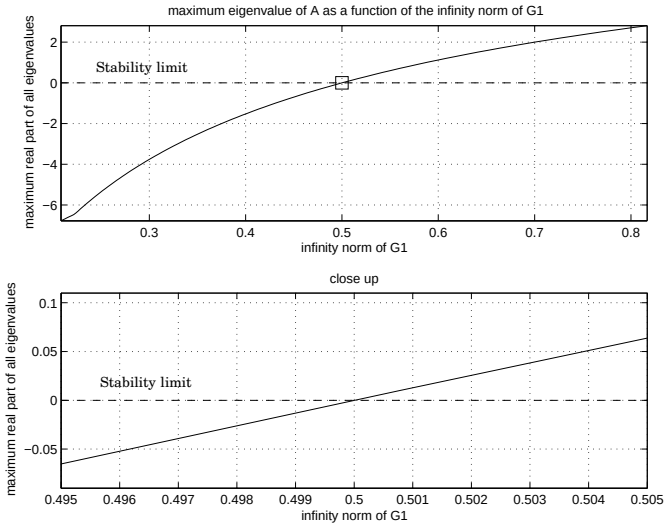

Figure 3.14 Maximum real part of all eigenvalues in the interconnected closed system as a function of $||G_\varepsilon||_\infty$

close to the stability limit. The limit is somewhat higher than the stability limit in Figure 3.10 which was derived in Matlab. This is most likely due to the fact that the Dymola model automatically models behavior of higher complexity than the Matlab model used to obtain Figure 3.10. As an example, forces are present in all directions in the Dymola model whereas in the Matlab model all forces act in the moving direction. See Figure 3.17.

The main features of the Matlab and Dymola models are also the same. The stability limit for the closed chain is constant and independent of the number of cars. In the open chain case the stability limit decreases as the number of cars increase.

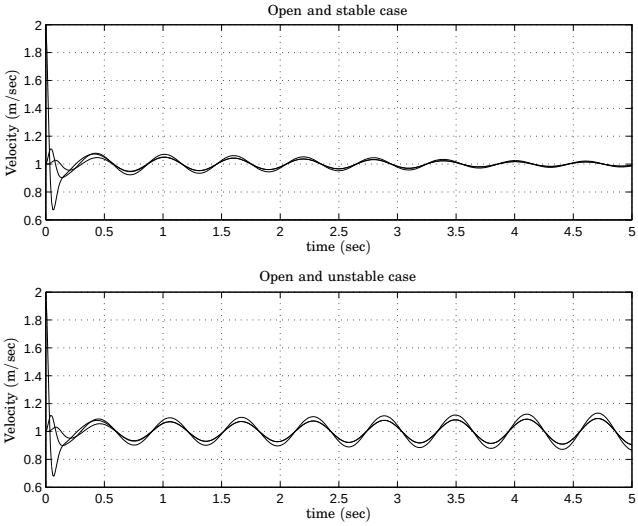

Figure 3.15 Upper plot: An open and stable chain of three cars with $||G_\varepsilon||_\infty = 0.74166$. Upper plot: An open and unstable chain of three cars with $||G_\varepsilon||_\infty = 0.7855$.

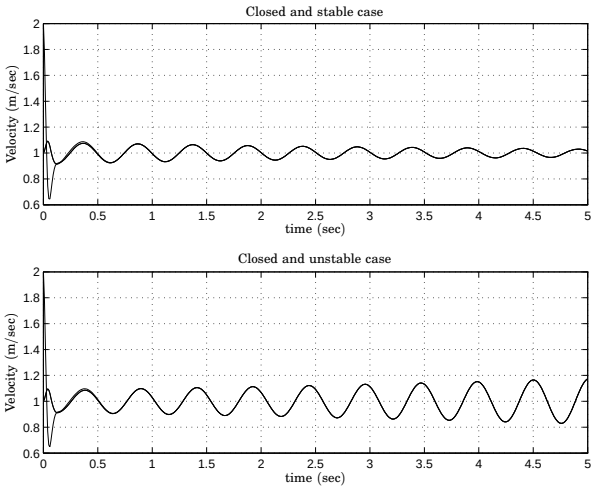

Figure 3.16 Upper plot: An closed and stable chain of three cars with $||G_\varepsilon||_\infty = 0.54197$. Upper plot: An closed and unstable chain of three cars with $||G_\varepsilon||_\infty = 0.55989$.

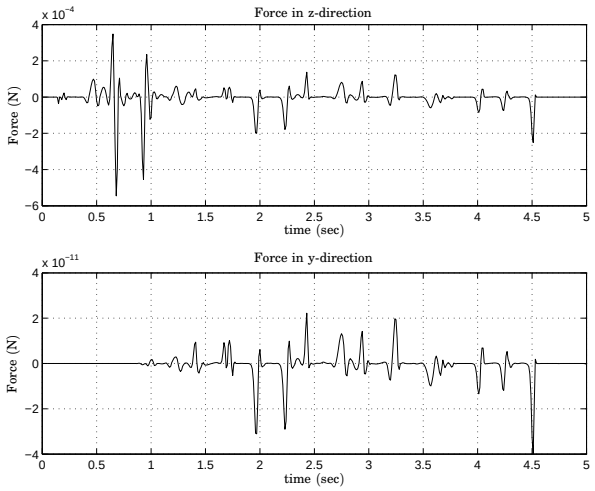

Figure 3.17 In Dymola simulations forces are also present in directions other than the moving direction. Upper plot: Force in y-direction. Lower plot: Force in z-direction. Both plots were obtained from the same simulation as Figure 3.15.

4. Conclusions

4.1 Problems and remarks

In the course of work some simplifications have been made that are not compatible with the actual conditions. The problems associated with these simplifications are listed below.

- All cars are assumed to have continuous contact with LIMs. This will not be true as it is assumed that the LIMs can be spread sparsely on the straight sections of the track. Accordingly the number of LIMs will be lower than the number of cars in these sections. In the transition region the distance between the LIMs will be closer. Furthermore, the maximum capacity of a LIM can only be used when the whole reactor disc of a car covers it. Figure 4.1 shows the capability of applying force on a car as it passes over the LIMs.

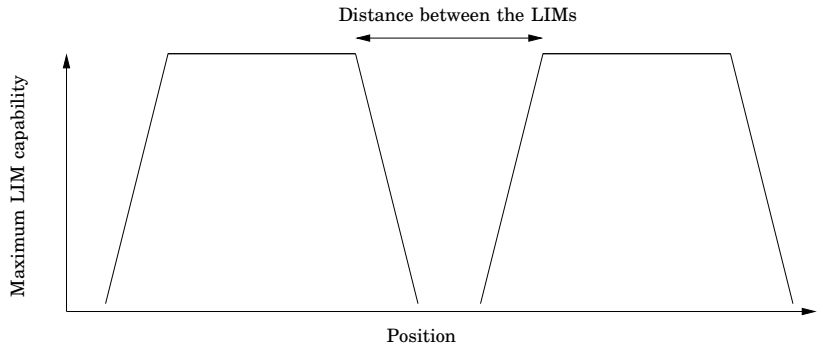

Figure 4.1 Capability of applying force on a car as it passes over the LIMs.

- The LIMs have been assumed to have infinite capacity. In the actual case, the maximum force that can be provided by a LIM is approximately 1000 N. This is of course a major issue since even for a small deviation in car velocity the control force takes very high values. See Figure 4.2 where a deviation of 1 m/sec is given to a car in a small chain.

Furthermore there are some other aspects that should be noticed.

- In order to apply theorem 3.1 as a string stability criteria, the controllers that are to operate in the transition zone have to keep the force against the rail constant and also make $||G_\varepsilon||_\infty$ sufficiently small. If the requirement on $||G_\varepsilon||_\infty$ is not met the chain can not be assumed to be broken and string stability can not be guaranteed.
- In this report the feedback signals associated with the car positioning are assumed to be continuous. In the actual case there will be sensors along the track at given positions. When a car passes a sensor, it will

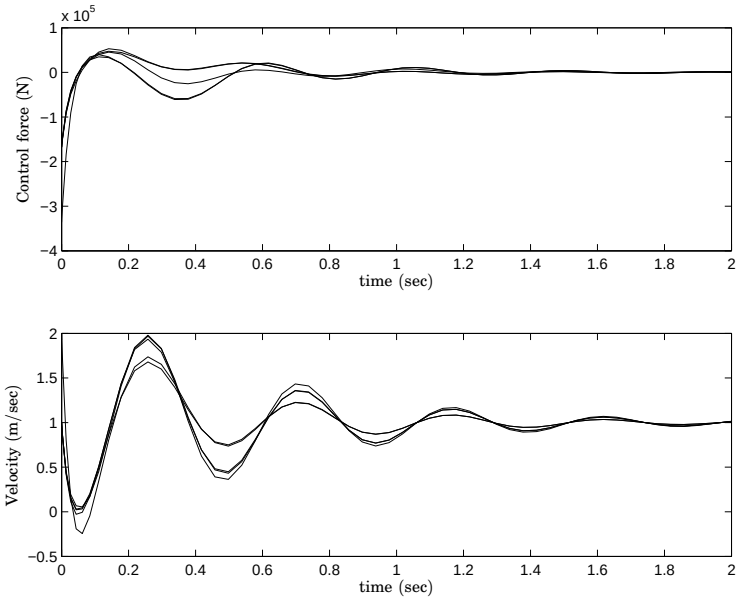

Figure 4.2 Simulation plot of a section of five cars where the first car has a deviation in velocity of 1 m/sec. $||G_\varepsilon||_\infty = 0.425$ between all cars. Note that the amplitude of the control signal is very high.

generate an impulse. The states of the car can then be reconstructed by using information from these impulses.

4.2 Suggestions for further development

- In order to simplify the control in the transition zone LIMs should be placed as in Figure 4.3. Then the central LIM will only affect the car along the x-direction. The two side LIMs should be controlled with an inner loop in order to only provide torque. Given these LIM placements the problem of reducing backlash effects and the problem of minimizing $||G_\varepsilon||_\infty$ can be separated.

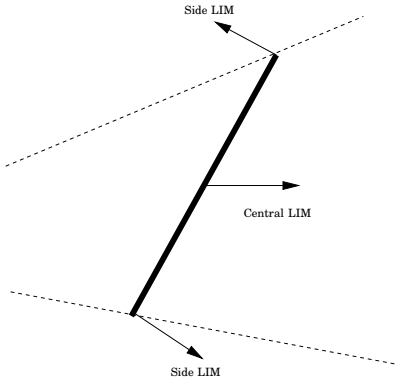

Figure 4.3 LIM placement that simplifies the control problem in the transition region.

A. Dymola models

A.1 Midi models

The midi models refer to single car-, distance beam-, LIM- and rail models. These models are described below and have been designed in cooperation with the Nowait Transit project group. The car consists of a main beam with two connecting points located on both ends. The connecting points are meant to be coupled with the rails and distance beams. The LIM forces are assumed to act in a direction of the rails. Figure A.1 shows how Midi models put together, constitute a car with controlled velocity on a track. The Modelica code associated with these models can be provided on request.

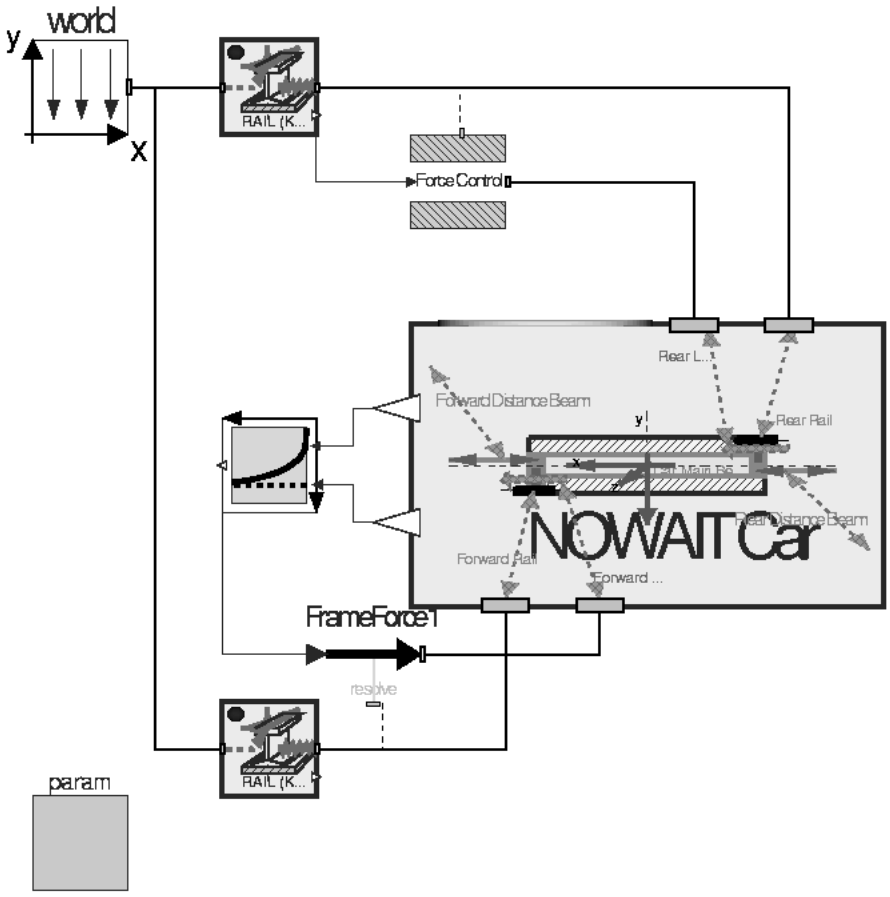

Figure A.1 A Nowait Transit car on a track.

Diagrams

The Nowait Transit Car Figure A.2 shows the components and connections of the car model.

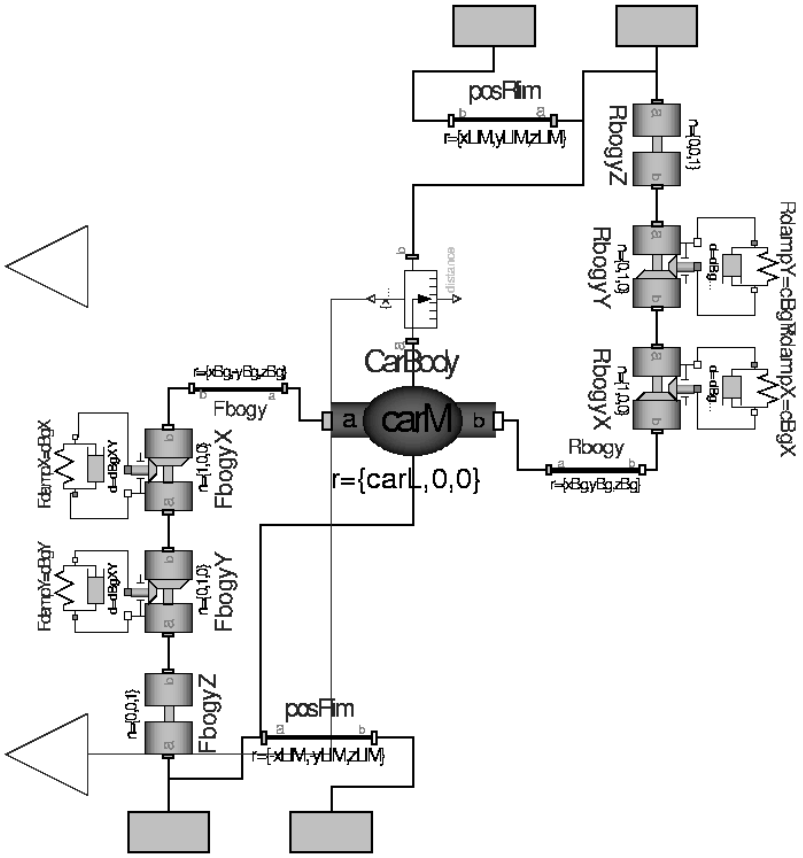

Figure A.2 Components and connections that constitute the Nowait Transit car

REMARK A.1
The two out-ports on the left side of Figure A.2 are used for feedback of car velocity and distance in x- and y-direction between the two ends of the car. □

The Nowait Transit Distance beam The distance beam components are shown in Figure A.3.

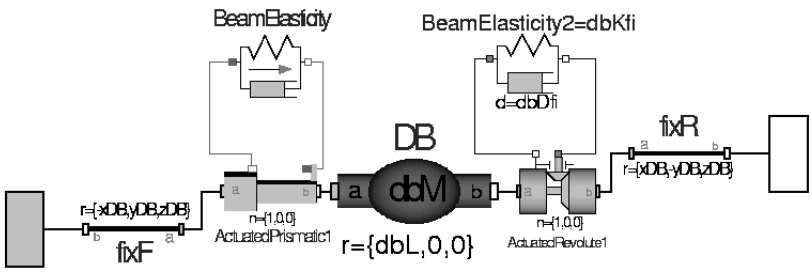

Figure A.3 Components and connections that constitute the Nowait Transit distance beam

The Nowait Transit Rail The rail components and connections are shown in Figure A.4.

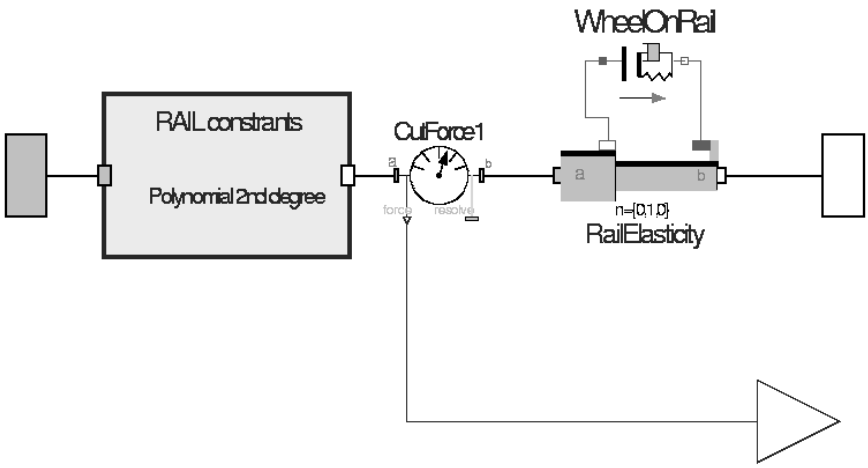

Figure A.4 Components and connections that constitute the Nowait Transit rail

REMARK A.2
The WheelOnRail component attached to RailElasticity in Figure A.4 models the backlash between the end of the car and the rail. □

Track The information about the track is available only in the component called *RAIL constraint*. This model is described in Figure A.5.

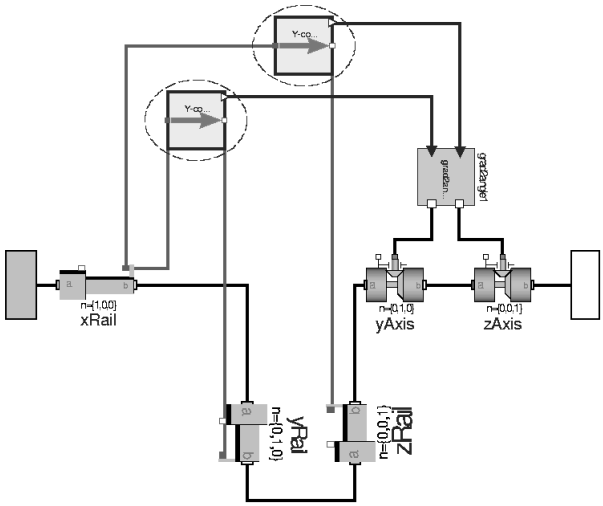

Figure A.5 Components and connections that constitute the model containing track information.

REMARK A.3
The track generators (encircled in Figure A.5) produce the coordinates and the angles of the rails as a function of the cars end positions. □

The controller The control components and connections are shown in Figure A.6.

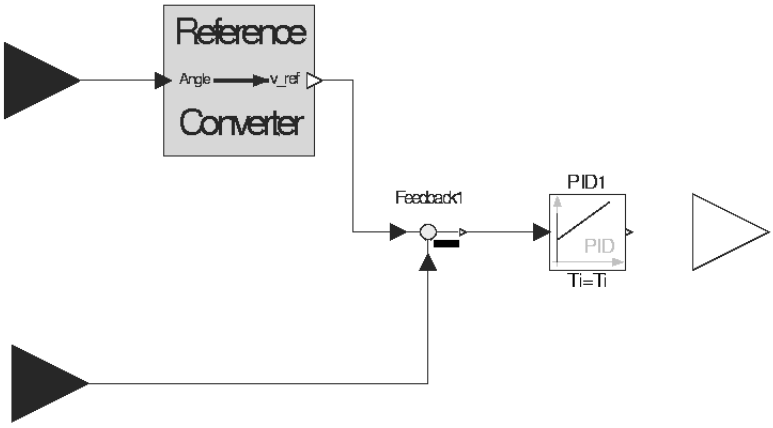

Figure A.6 Components and connections that constitute the controller

REMARK A.4
The reference generator in Figure A.6 produces the velocity reference for a car as a function of it's folding angle. □

A.2 Macro models

Macro models refer to models that contain interconnected cars. The Macro models in Dymola have been implemented in order to validate Theorem 3.1 and the indication of the closed chain stability in Section 3.4. The Modelica code associated with the models described can be provided on request.

Diagrams

Broken chain In the model in Figure A.7 the cars constitute a open chain.

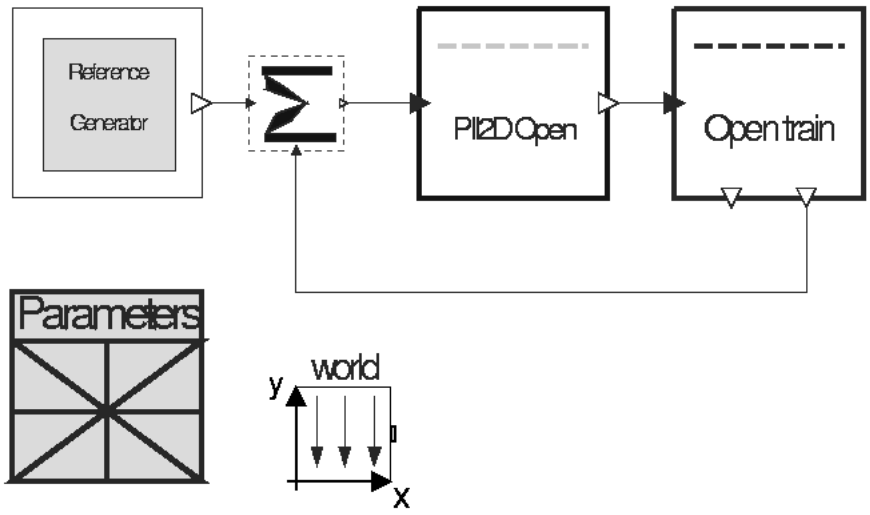

Figure A.7 Diagram of model where the cars constitute a open chain.

Closed Chain In the model in Figure A.8 the cars constitute a closed chain.

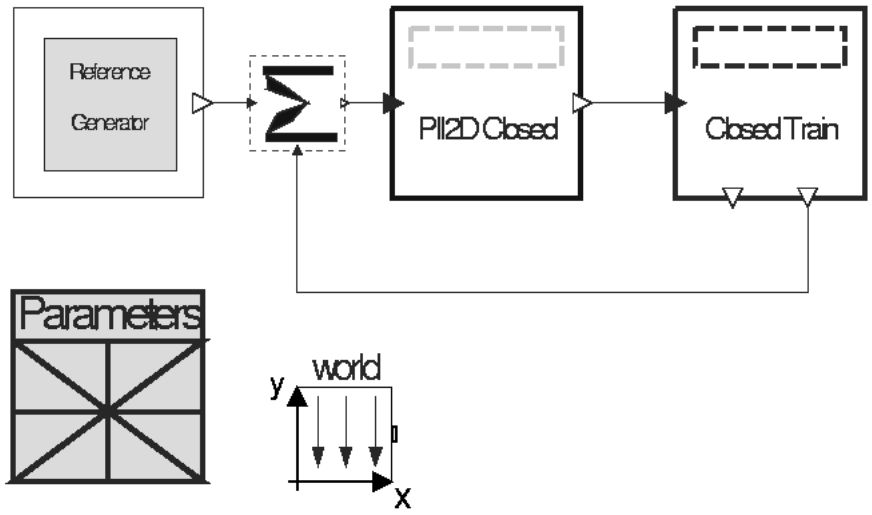

Figure A.8 Diagram of model where the cars constitute a closed chain.

B. Matlab scripts and Simulink Models

Some of the Simulink models concerning the Midi models are provided in this section. Matlab code for both Midi and Macro models can be provided on request.

All models in this appendix are force controlled. The Simulink model for the model described in Section 2.1 is shown in Figure B.1. The controlled model is displayed in Figure B.2.

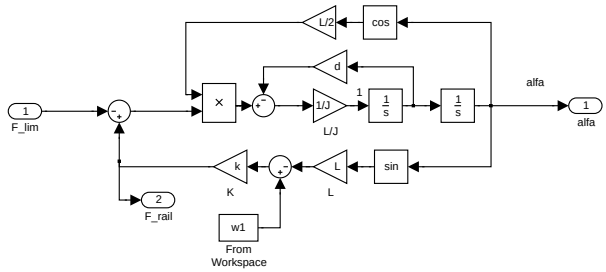

Figure B.1 Model of a car on the rail.

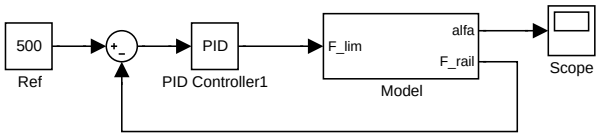

Figure B.2 The model controlled with a PID controller.

C. Converting rail data to functions

If the samples of the track are interpolated by raw spline or polynomial techniques the resulting functions will carry a high complexity.

In the first case, and for n samples, n different polynomial functions (splines) will have to be used. Since simulation of basic mechanical components in Dymola uses derivatives up to second order and since the Nowait Transit models sometimes derivate a signal, the splines have to be C^3-continuous. To achieve C^3-continuity the splines have to be of order 4. This means that the program has to keep track of $32n$ coefficients in order to describe the two tracks in the space and the high complexity will reduce the simulation performance of our model.

In the second case, using just a single polynomial, the order of the polynomial for each track will be somewhere between 40 and 60. The high order is required to achieve sufficient accuracy since even a small deviation from the ideal track will give rise to high forces. Calculation in 2 directions for each rail along every point on the x-axis interval will also reduce the simulation performance.

In order to attain faster simulation results the interpolation method will rely on a polynomial and spline interpolation hybrid-technique. The idea is to use just a few polynomials of relatively low order and connect these polynomials by a single spline such that the C^3-continuity requirement is fulfilled.

C^q-continuity will impose the following boundary conditions on the spline

$$\frac{d^k s(t^-)}{dt^k} = \frac{d^k p^-(t^+)}{dt^k} \tag{C.1}$$

$$\frac{d^k s(t^+)}{dt^k} = \frac{d^k p^+(t^+)}{dt^k} \tag{C.2}$$

where $k = 0, 1, \ldots, q$. p^+, p^- are the polynomials connecting to the left and right boundary of the spline respectively, and t^+, t^- are the points along the x-axis where the connections are made.
C^q-continuity gives rise to $2(q+1)$ conditions on a spline. A spline of order r contains $r+1$ unknowns. To satisfy the continuity conditions, $r+1 = 2(q+1)$, which means $r = 2q+1$. Since $q = 3$ the spline will be given by:

$$s(t) = a_1(t-t^-)^7 + a_2(t-t^-)^6 + a_3(t-t^-)^5 + a_4(t-t^-)^4 + a_5(t-t^-)^3 + a_6(t-t^-)^2 + a_7(t-t^-) + a_8$$

where $t \in [t^-, t^+]$.

Condition (C.1) automatically results in

$$\begin{aligned} a_6 &= \frac{1}{3}\frac{d^3p^-(t^-)}{dt^3} \\ a_6 &= \frac{1}{2}\frac{d^2p^-(t^-)}{dt^2} \\ a_7 &= \frac{dp^-(t^-)}{dt} \\ a_8 &= p^-(t^-). \end{aligned}$$

Subsequently, using condition (C.2) and defining $h = t^+ - t^-$, yields the following equation system

$$\begin{aligned} a_1h^7 + a_2h^6 + a_3h^5 + a_4h^4 &= p^+(t^+) - a_5h^3 - a_6h^2 - a_7h - a_8 \\ 7a_1h^6 + 6a_2h^5 + 5a_3h^4 + 4a_4h^3 &= \frac{dp^+(t^+)}{dt} - 3a_5h^2 - 2a_6h - a_7 \\ 42a_1h^5 + 30a_2h^4 + 20a_3h^3 + 12a_4h^2 &= \frac{d^2p^+(t^+)}{dt^2} - 6a_5h - 2a_6 \\ 210a_1h^4 + 120a_2h^3 + 60a_3h^2 + 24a_4h &= \frac{d^3p^+(t^+)}{dt^3} - 6a_5 \end{aligned}$$

which can be solved for a_1, a_2, a_3 and a_4.

The function for the upper rail in y-direction is plotted in Figure C.1 together with its derivatives.

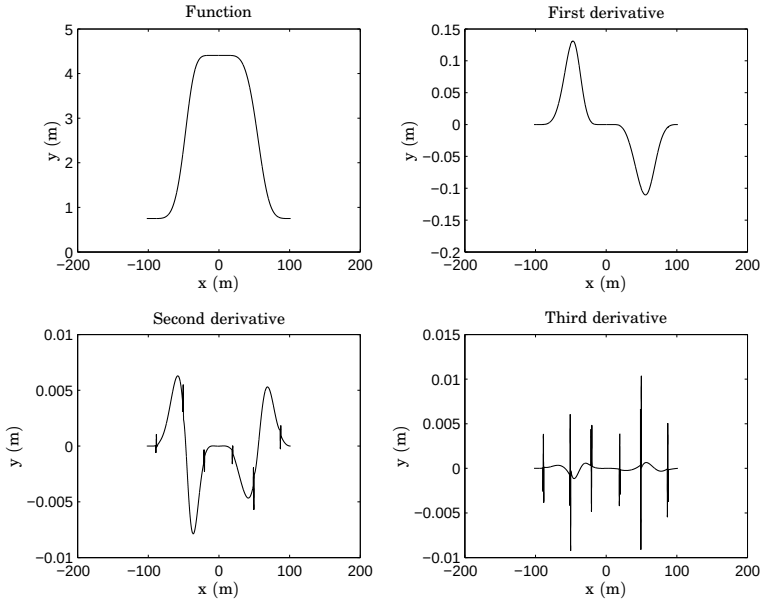

Figure C.1 The track function for the upper rail in y-direction and its derivatives.

References

[1] D. Swaroop and J. K. Hedrick, "String Stability of Interconnected Systems", *IEEE Transactions on Automatic Control*, vol 41, no 3, 1996, pp 349-357.

[2] D. Yankiev and I. Kanellakopoulos, "A Simplified Framework for String Stability Analysis in AHS", *Proc. of the 13th IFAC World Congress*, vol Q, 1996, pp 177-182

[3] C.Y. Liang and H. Peng, "String Stability of Adaptive Cruise Controlled Vehicles", Department of Mechanical Engineering and Applied Mechanics, University of Michigan, 2000.

[4] R. Rajamani and S.E. Shaladover, "An experimental comparative study of autonomous and co-operative vehicle-follower control systems", Department of Mechanical Engineering, University of Minnesota, May 200.

[5] S. Sheikholeslam and C.A. Desoer, "Longitudal Control of a Platoon of Vehicles with no Communication of Lead Vehicle Information: A System Level Study", *IEEE Transactions of on Vehicular Technology*, vol 42, no 3, pp 546-554.

[6] S. Sheikholeslam and C.A. Desoer, "Longitudal Control of a Platoon of Vehicles", Department of Electrical Engineering and Computer Science, University of California, Berkeley.

[7] M.E. Khatir and E.J. Davidson, "Bounded Stability and Eventual String Stability of a Large Platoon of Vehicles Using Non-Identical Controllers", Department of Electrical and Computer Engineering, University of Toronto.